

Confinement Free Energy of Flexible Polyelectrolytes in Spherical Cavities

Rajeev Kumar and M.Muthukumar *

*Dept. of Polymer Science & Engineering,
Materials Research Science & Engineering Center,
University of Massachusetts, Amherst, MA-01003, USA.*

ABSTRACT

A weakly charged flexible polyelectrolyte chain in a neutral spherical cavity is analyzed using self-consistent field theory (SCFT) within an explicit solvent model. Assuming the radial symmetry for the system, it is found that the confinement of the chain leads to creation of a charge density wave along with the development of a potential difference across the center of cavity and the surface. We show that the solvent entropy plays an important role in the free energy of the confined system. For a given radius of the spherical cavity and fixed charge density along the backbone of the chain, solvent and small ion entropies dominate over all other contributions when chain lengths are small. However, with the increase in chain length, chain conformational entropy and polymer-solvent interaction energy also become important. Our calculations reveal that energy due to electrostatic interactions plays a minor role in the free energy. Furthermore, we show that the total free energy under spherical confinement is not extensive in the number of monomers. Results for the osmotic pressure and mean activity coefficient for monovalent salt are presented. We demonstrate that fluctuations at one-loop level lower the free energy and corrections to the osmotic pressure and mean activity coefficient of the salt are discussed. Finite size corrections are shown to widen the range of validity of the fluctuation analysis.

* To whom any correspondence should be addressed, Email : muthu@polysci.umass.edu

I. INTRODUCTION

Polyelectrolytes are ubiquitous in nature and exhibit rich behavior. In the past, a great deal of theoretical^{1,2,3,4,5,6,7,8,9,10} and experimental efforts^{11,12,13,14,15,16} have been made in understanding their characteristics in solutions with concentrations ranging from dilute to concentrated. One of the remarkable discoveries in the last century is the theory of simple electrolytes made by Debye and Hückel¹⁷, where electrostatic interactions get screened (colloquially referred to as the Debye screening). Similar phenomenon was shown to be present in the case of neutral polymers, where monomers interact by short range excluded volume interaction potential (known as Edward's screening¹⁸). In the case of polyelectrolytes, both kinds of screening effects are present and their coupling via the concept of double screening was introduced by Muthukumar⁶, and the behavior of polyelectrolyte solutions was described in terms of these screening phenomena. As a result, different concentration regimes in polyelectrolyte solutions were predicted and verified experimentally^{11,12}.

However, most of the computer and real-world experiments involve finite volume, where boundary effects play a significant role and can not be ignored. Recently, there has been a resurgence of interest in studying polymers within confined domains^{19,20,21,22,23,24,25,26,27,28,29,30}. Unlike neutral polymers, little is known about the physics of polyelectrolytes under confinement, a situation realized in liposome-mediated delivery of macromolecules to the cells¹⁹, translocation experiments involving RNA/DNA^{20,21}, synthetic polyelectrolytes²² etc. Underlying physics in these experiments is governed by the confinement effects on a *single* polyelectrolyte chain. Physically, confinement forces interaction among the monomers and the conformational entropy of the chain gets lowered due to less number of conformational states available to the chain. If small components like salt ions and solvent molecules are also present in addition to the polymer, then translational entropy of these components gets diminished, making confinement a thermodynamically unfavorable process. Quantitative estimates of these confinement effects are desirable. Recently, a quantitative description of the finite size corrections³¹ to free energy for electrolytic systems has been presented. The analog of these calculations for polyelectrolyte systems has not been attempted yet and is one of the goals of this study.

In this study, we focus on a single polyelectrolyte chain confined in a neutral spherical cavity and use radial symmetry to obtain the mean field results. This theoretical model

is pertinent in understanding many important physical processes. Few promising applications of this model are the computation of free energy barriers for the chain to move out of the confining space, osmotic pressure of polyelectrolytes, etc. To start with, we consider a situation where inner and outer dielectric constants of medium are different (say ϵ_i and ϵ_o , respectively). For this situation, the electrostatic potential is to be calculated using continuity of electrostatic potential and normal component of displacement vector at the boundary. It turns out that these boundary conditions are equivalent to a continuous dielectric medium (of dielectric constant ϵ_i everywhere) with charges confined within the boundary of sphere for the *radially symmetric globally electroneutral* system. In other words, dielectric mismatch effects disappear due to the use of radial symmetry. We must point out that radial symmetry is strictly valid only at the mean field level and fluctuations break this symmetry. In the concentrated regime, we have been able to compute the fluctuation contributions without recourse to radial symmetry.

Unlike cylindrical²³ and rectangular^{23,24} confinements, a single self-avoiding chain in a spherical cavity has been shown to be a polymer solution problem^{18,25,26,27,32,33} with different degrees of confinements corresponding to different concentration regimes as seen in polymer solution theories. We are here interested in estimating different thermodynamic contributions to the free energy of confined polyelectrolytic system. Computing these contributions using simulations is a formidable task. However, self-consistent field theory (SCFT) presents a faster and an accurate way to address this problem. SCFT allows us to explore the role of confinement in free energy at the mean field level (also known as the saddle point approximation) and then capture the role of fluctuations by expanding free energy functional around the mean field solution (one-loop calculations). Unlike earlier studies on single neutral chain²⁸, we use “explicit solvent model”, which captures solvent entropy in a more realistic way. At the mean field level, free energy for a self-avoiding chain under strong confinement (in vacuum) has been shown to be proportional to $w\bar{\rho}_p^2\Omega$, where w is a measure of the strength of excluded volume interactions, $\bar{\rho}_p$ is monomer density and Ω is the volume of the cavity. Remarkably, same proportionality is exhibited by polymer solution theories^{18,32} in the concentrated regime. However, at *low* polymer concentrations (i.e. dilute and semi-dilute regime), fluctuations around the saddle point solution become important and saddle point approximation breaks down. In that case, non-perturbative techniques have to be devised to compute the correct free energy. In this work, we explore the free

energy in the concentrated regime, when radius of gyration of the chain is comparable to the radius of the cavity and mean field theory is still applicable.

Dividing the free energy into energetic and entropic parts using thermodynamic arguments, we have identified the role of individual components. Moreover, one loop calculations provide insight about the corrections to the bulk expressions from fluctuation effects in the concentrated regime. For a globally neutral system with only small ions (i.e. without polyelectrolyte) inside a neutral cavity, local electroneutrality is the equilibrium state. In contrast, local electroneutrality is violated in the presence of a polyelectrolyte chain due to the depletion effects present in the system. We have studied the resulting monomer and charge density distribution for different sets of relevant parameters of the problem. To link with the experiments, we have computed the osmotic pressure and mean activity coefficient for monovalent salt.

This paper is organized as follows: theory is presented in Sec. II; calculated results and conclusions are presented in Sec. III and IV, respectively.

II. THEORY

A. Self-consistent field theory

We consider a spherical cavity of radius R containing a single flexible polyelectrolyte chain of total N Kuhn segments, each with length b . The polyelectrolyte chain is represented as a continuous curve of length Nb and an arc length variable t is used to represent any segment along the backbone. We assume that there are n_c monovalent counterions (positively charged) released by the chain (and assuming that the chain is negatively charged for the sake of specificity). In addition, there are n_γ ions of species γ ($= +, -$) coming from added salt (in volume $\Omega = 4\pi R^3/3$) so that the whole system is globally electroneutral. Let Z_j be the valency (with sign) of the charged species of type j . Moreover, we assume that there are n_s solvent molecules (satisfying the incompressibility constraint) present in the cavity and for simplicity, each solvent molecule occupies a volume (v_s) same as that of the monomer (i.e. $v_s \equiv b^3$). Subscripts $p, s, c, +$ and $-$ are used to represent monomer, solvent, counterion from polyelectrolyte, positive and negative salt ions, respectively. Degree of ionization of the chain is taken to be α and we consider smeared charge distribution so that each of

the segments carries a charge $e\alpha Z_p$, where e is the electronic charge.

If electrostatic interactions between solvent molecules and small ions are ignored, the partition function for the system can be written as

$$\begin{aligned} \exp\left(-\frac{F}{k_B T}\right) &= \frac{1}{\prod_j n_j!} \int D[\mathbf{R}] \int \prod_j \prod_{m=1}^{n_j} d\mathbf{r}_m \exp\left\{-\frac{3}{2b} \int_0^{Nb} dt \left(\frac{\partial \mathbf{R}(t)}{\partial t}\right)^2\right. \\ &\quad -\frac{1}{2b^2} \int_0^{Nb} dt \int_0^{Nb} dt' V_{pp}[\mathbf{R}(t) - \mathbf{R}(t')] - \frac{1}{b} \sum_j \sum_{m=1}^{n_j} \int_0^{Nb} dt V_{pj}[\mathbf{R}(t) - \mathbf{r}_m] \\ &\quad \left. -\frac{1}{2} \sum_j \sum_a \sum_{m=1}^{n_j} \sum_{p=1}^{n_a} V_{ja}[\mathbf{r}_m - \mathbf{r}_p]\right\} \prod_{\mathbf{r}} \delta(\hat{\rho}_p(\mathbf{r}) + \hat{\rho}_s(\mathbf{r}) - \rho_0) \end{aligned} \quad (1)$$

where $\mathbf{R}(t)$ represents the position vector for t^{th} segment and subscripts $j, a = s, c, +, -$. In the above expression, it is understood that the factor of $1/2$ in the last term inside the exponent is there, only when $j = a$. In Eq. (1), $k_B T$ is the Boltzmann constant times absolute temperature. $V_{pp}(\mathbf{r})$, $V_{ss}(\mathbf{r})$ and $V_{ps}(\mathbf{r})$ represent monomer-monomer, solvent-solvent and monomer-solvent interaction energies, respectively, when the interacting species are separated by distance $r = |\mathbf{r}|$ and are given by

$$V_{pp}(\mathbf{r}) = w_{pp}\delta(\mathbf{r}) + \frac{Z_p^2 e^2 \alpha^2}{\epsilon k_B T} \frac{1}{r} \quad (2)$$

$$V_{ss}(\mathbf{r}) = w_{ss}\delta(\mathbf{r}) \quad (3)$$

$$V_{ps}(\mathbf{r}) = w_{ps}\delta(\mathbf{r}). \quad (4)$$

Here, w_{pp} , w_{ss} and w_{ps} are the excluded volume parameters, which characterize the short range excluded volume interactions between monomer-monomer, solvent-solvent and monomer-solvent, respectively. $\delta(\mathbf{r})$ is the three dimensional Dirac delta function and ϵ is position independent effective dielectric constant of the medium (in units of $4\pi\epsilon_o$, where ϵ_o is the permittivity of vacuum). Delta functions involving microscopic densities enforce incompressibility condition at all points in the system (ρ_0 being total number density of the system). Interactions between polyelectrolyte segments and small ions as represented by V_{pj} , are given by

$$V_{pj}(\mathbf{r}) = \frac{Z_p Z_j e^2 \alpha}{\epsilon k_B T} \frac{1}{r} \quad \text{for } j = c, +, -. \quad (5)$$

In writing the interaction energies between polyelectrolyte segments and small ions, we have taken small ions to be point charges so that they have zero excluded volume and

interactions are purely electrostatic in nature. In the point charge limit for the small ions, interaction between two small ions is written as

$$V_{ja}(\mathbf{r}) = \frac{Z_j Z_a e^2}{\epsilon k_B T} \frac{1}{r} \quad \text{for } j, a = c, +, -. \quad (6)$$

Following the standard protocol³⁴ to obtain saddle point equations (see Appendix A), the Poisson-Boltzmann equation for electric potential gets coupled to the well-known modified diffusion equation for chain connectivity. In particular, the saddle point equations are given by

$$\phi_p(\mathbf{r}) = \chi_{ps} b^3 \rho_s(\mathbf{r}) + \eta(\mathbf{r}) \quad (7)$$

$$\phi_s(\mathbf{r}) = \chi_{ps} b^3 \rho_p(\mathbf{r}) + \eta(\mathbf{r}) \quad (8)$$

$$\rho_p(\mathbf{r}) = \frac{1}{Q_p} \int_0^N ds q(\mathbf{r}, s) q(\mathbf{r}, N - s) \quad (9)$$

$$\rho_s(\mathbf{r}) = \frac{n_s}{Q_s} \exp[-\phi_s(\mathbf{r})] \quad (10)$$

$$\rho_p(\mathbf{r}) + \rho_s(\mathbf{r}) = \rho_0 \quad (11)$$

$$\rho_j(\mathbf{r}) = \frac{n_j}{Q_j} \exp[-Z_j \psi(\mathbf{r})] \quad \text{for } j = c, +, - \quad (12)$$

$$\nabla_{\mathbf{r}}^2 \psi(\mathbf{r}) = -4\pi l_B \left[\sum_{j=c,+,-} Z_j \rho_j(\mathbf{r}) + Z_p \alpha \rho_p(\mathbf{r}) \right]. \quad (13)$$

These equations are equivalent to those derived by Shi and Noolandi³⁵, and Wang³⁶ *et al.*, although the method of derivation is different as briefly outlined in Appendix A. In these equations, $\rho_\beta(\mathbf{r})$ and $\phi_\beta(\mathbf{r})$ are respectively the macroscopic number density and the field experienced by particles of type β , due to excluded volume interactions. All charged species experience electrostatic potential represented by $\psi(\mathbf{r})$ above. Note that $\psi(\mathbf{r})$ in above equations is dimensionless (in units of $k_B T/e$) and l_B depicts the Bjerrum length defined as $l_B = e^2/\epsilon k_B T$. Moreover, χ_{ps} is the dimensionless Flory's chi parameter and $\rho_0 = (N + n_s)/\Omega = 1/b^3$. Also, $\eta(\mathbf{r})$ is the well-known pressure field introduced to enforce the incompressibility constraint. The function $q(\mathbf{r}, s)$ is the probability of finding segment s at location \mathbf{r} , when starting end of the chain can be anywhere in space, satisfying the modified diffusion equation³⁷

$$\frac{\partial q(\mathbf{r}, s)}{\partial s} = \left[\frac{b^2}{6} \nabla_{\mathbf{r}}^2 - \{Z_p \alpha \psi(\mathbf{r}) + \phi_p(\mathbf{r})\} \right] q(\mathbf{r}, s), \quad s \in (0, N). \quad (14)$$

Also, Q_β represents the partition function for the particle of type β in the field experienced by it, given by

$$Q_s = \int d\mathbf{r} \exp[-\phi_s(\mathbf{r})] \quad (15)$$

$$Q_p = \int d\mathbf{r} q(\mathbf{r}, N) \quad (16)$$

$$Q_j = \int d\mathbf{r} \exp[-Z_j \psi(\mathbf{r})] \quad \text{for } j = c, +, -. \quad (17)$$

Using the above equations, approximated free energy at the extremum (saddle point approximation) is given by

$$\begin{aligned} \frac{F^*}{k_B T} = & \frac{F_0}{k_B T} - \chi_{ps} b^3 \int d\mathbf{r} \rho_p(\mathbf{r}) \rho_s(\mathbf{r}) + \frac{1}{8\pi l_B} \int d\mathbf{r} \psi(\mathbf{r}) \nabla_{\mathbf{r}}^2 \psi(\mathbf{r}) - \ln Q_p + \sum_j n_j \left[\ln \frac{n_j}{Q_j} - 1 \right] \\ & - \rho_0 \int d\mathbf{r} \eta(\mathbf{r}), \end{aligned} \quad (18)$$

where $j = s, c, +, -$ and $F_0/k_B T = \frac{\rho_0}{2} (N w_{pp} + n_s w_{ss})$ is the self-energy contribution arising from excluded volume interactions. Using thermodynamic arguments³⁸ and assuming dielectric constant (ϵ) to be independent of temperature (T), the free energy (Eq. (18)) is divided into enthalpic contributions due to excluded volume, electrostatic interactions and entropic part due to small ions, solvent molecules and the polyelectrolyte chain. Denoting these contributions by $E_w, E_e, S_{ions}, S_{solvent}$ and S_{poly} , respectively, the free energy is written as

$$\frac{F^* - F_0}{k_B T} = \frac{E_w}{k_B T} + \frac{E_e}{k_B T} - \frac{T(S_{ions} + S_{solvent} + S_{poly})}{k_B T} \quad (19)$$

$$\frac{E_w}{k_B T} = \chi_{ps} b^3 \int d\mathbf{r} \rho_p(\mathbf{r}) \rho_s(\mathbf{r}) + \rho_0 \int d\mathbf{r} \eta(\mathbf{r}) \quad (20)$$

$$\frac{E_e}{k_B T} = \frac{1}{2} \int d\mathbf{r} \psi(\mathbf{r}) \left(\sum_{j=c,+, -} Z_j \rho_j(\mathbf{r}) + Z_p \alpha \rho_p(\mathbf{r}) \right) \quad (21)$$

$$\begin{aligned} -\frac{T S_{ions}}{k_B T} = & - \sum_{j=c,+, -} \left[n_j \ln Q_j + \int d\mathbf{r} Z_j \rho_j(\mathbf{r}) \psi(\mathbf{r}) \right] + \sum_{j=c,+, -} n_j [\ln n_j - 1] \\ = & \sum_{j=c,+, -} \int d\mathbf{r} \rho_j(\mathbf{r}) \{ \ln [\rho_j(\mathbf{r})] - 1 \} \end{aligned} \quad (22)$$

$$\begin{aligned} -\frac{T S_{solvent}}{k_B T} = & - \left[n_s \ln Q_s + \int d\mathbf{r} \rho_s(\mathbf{r}) \phi_s(\mathbf{r}) \right] + n_s [\ln n_s - 1] \\ = & \int d\mathbf{r} \rho_s(\mathbf{r}) \{ \ln [\rho_s(\mathbf{r})] - 1 \} \end{aligned} \quad (23)$$

$$-\frac{TS_{poly}}{k_B T} = -\ln Q_p - \int d\mathbf{r} [\{Z_p \alpha \psi(\mathbf{r}) + \phi_p(\mathbf{r})\} \rho_p(\mathbf{r}) + \rho_0 \eta(\mathbf{r})]. \quad (24)$$

So far, we have presented a general field theoretical treatment for a single polyelectrolyte chain and haven't considered confinement. We study the role of confinement by solving Eqs. (7-13) under a particular set of boundary conditions and constraints, which are presented in the next section. Also, the limits of volume integral in Eqs. (19-24) vary over the volume of confining spherical cavity.

B. Boundary Conditions and Constraints

The above treatment leads to coupling of non-linear Poisson-Boltzmann equation with modified diffusion equation. Both of these equations are second order differential equations and hence, two conditions are required for each, in order to obtain a unique solution. In addition, for s dependent diffusion equation, an initial condition is needed to start the computations. To solve these equations, we exploit the assumed spherical symmetry of the system so that $q(\mathbf{r}, s) \rightarrow q(r, s)$ and the Laplacian is given by

$$\nabla_{\mathbf{r}}^2 = \frac{1}{r^2} \frac{\partial}{\partial r} \left(r^2 \frac{\partial}{\partial r} \right) \quad (25)$$

Due to symmetry of the system, additional requirements need to be fulfilled by the solution. Here, we summarize all these conditions:

$$\text{Boundary Conditions : } \frac{\partial \psi(r)}{\partial r} \Big|_{r=R} = 0, q(R, s) = 0 \quad \text{for all } s \quad (26)$$

$$\text{Initial Conditions : } q(r, 0) = 1 \quad \text{for all } r \neq R \quad (27)$$

$$\text{Symmetry Conditions: } \frac{\partial \psi(r)}{\partial r} \Big|_{r=0} = \frac{\partial q(r, s)}{\partial r} \Big|_{r=0} = 0 \quad \text{for all } s \quad (28)$$

Boundary and initial conditions for $q(r, s)$ correspond to the facts that (a) segments are excluded from boundary so probability of finding any segment at the boundary is zero and (b) the ends can be anywhere inside sphere. Symmetry condition for $q(r, s)$ is invoked because we are looking for a symmetrical solution of monomer density about the center without any discontinuity. Boundary condition and symmetry conditions for electrostatic potential are obtained by using the Gauss law at the boundary and the fact that net force experienced by an ion at the center of the sphere must be zero.

Along with the above initial and boundary conditions, solution of SCF equations need to be obtained under additional constraints due to the fixed number of monomers (N), ions (n_j) and global electroneutrality so that

$$Z_p \alpha N + Z_c n_c = 0, \quad Z_+ n_+ = -Z_- n_- = 0.6023 c_s \Omega, \quad (29)$$

where c_s is salt concentration in moles per liter (molarity) and Ω is in units of nm^3 .

C. Numerical Technique

We have solved SCF equations (Eqs. (7 - 14)) in real space using an explicit finite difference scheme for Poisson-Boltzmann-like equation (Eq. (13)) and the standard Crank-Nicolson³⁹ scheme for solving modified diffusion equation (Eq. (14)). Due to the use of properly normalized equations for densities, all the constraints mentioned earlier are always satisfied during the computation.

As the solution of SCF equations is invariant when an arbitrary constant is added to the fields, so this constant needs to be fixed in order to obtain a unique solution. Choice of fixing this constant depends on the numerical scheme used in solving the SCF equations. We simply choose $\psi(R) = 0$ and $\int d\mathbf{r} \eta(\mathbf{r}) = 0$. We must point out that any method of fixing this constant does not affect the densities but the free energy gets changed by a constant.

To realize the constraint $\int d\mathbf{r} \eta(\mathbf{r}) = 0$, $\frac{1}{\Omega} \int d\mathbf{r} \eta(\mathbf{r})$ is subtracted from the computed $\eta(\mathbf{r})$ at each iteration. This procedure leads to $\int d\mathbf{r} \eta(\mathbf{r}) = 0$ in the final solution. Also, all the integrals are evaluated by the standard Trapezoidal³⁹ rule and Broyden's method³⁹ is used to solve the set of non-linear equations.

D. Reference System

The choice of a reference system in free energy calculations depends on the physical quantity of interest. One of our goals in this study is to investigate the role of the polyelectrolyte chain in the free energy of the system. To study the role of the chain, the spherical cavity without any polymer (with small ions and solvent inside) is the appropriate choice.

In the absence of the chain, free energy becomes

$$\frac{F\{\bar{\rho}_p = 0\} - F_0\{N = 0\}}{k_B T} = \sum_{j=+,-,s} n_j \left[\ln \frac{n_j}{\Omega} - 1 \right]. \quad (30)$$

Note that in the absence of the chain, $n_s b^3 = \Omega$, due to the incompressibility condition.

E. Osmotic Pressure: Contact Value Theorem

Although we have computed the free energy of a confined chain, it is worthwhile to compute a physical observable, which is readily measurable experimentally. So, we have computed the osmotic pressure of a confined chain by carrying out the variation of free energy (Eq. (18)) with respect to the number of solvent molecules, but keeping the number of monomers and salt ions fixed (and taking care of the fact that volume has to be changed to alter the number of solvent molecules for the incompressible system under investigation here). The osmotic pressure is given by³³

$$\frac{\Pi b^3}{k_B T} = - \left[\frac{\delta}{\delta n_s} \left(\frac{F - F_0}{k_B T} \right)_{N, n_j} - \frac{\delta}{\delta n_s} \left(\frac{F - F_0}{k_B T} \right)_{N, n_j=0} \right], \quad (31)$$

where $j = c, +, -$. Within the saddle point approximation, $F = F^*$ and $(F^* - F_0)/k_B T = -n_s$ for pure solvent (i.e. when $N, n_j = 0$). Using the above formula, osmotic pressure comes out to be (within radial symmetry)

$$\begin{aligned} \frac{\Pi^*}{k_B T} = & \sum_{j=c,+, -} \rho_j(R^-) - \rho_p(R^-) - \ln \rho_s(R^-) + \frac{q(R^-, N)}{\int d\mathbf{r} q(\mathbf{r}, N)} \\ & - \chi_{ps} b^3 \rho_p^2(R^-) + \rho_e(R^-) \psi(R^-), \end{aligned} \quad (32)$$

where $\rho_e(R^-)$ is the total charge density (in units of electronic charge) at a point close to the surface of the cavity and \star in the superscript depicts the fact that saddle point approximation for the free energy has been used in deriving the result. Due to the coarse grained model used in studying the single chain, information at a length scale below Kuhn's segment length is not correctly captured by the model. So, R^- represents the point, which is at a distance of one Kuhn segment length from the surface. This point is well-discussed in the literature^{40,41} and will not be pursued further.

If we were to imagine a system, where densities and fields are constant (as in the concentrated bulk system), then the above expression simplifies to the well-known¹⁸ expression for the osmotic pressure of a homogeneous system (represented by Π_h^*)

$$\frac{\Pi_h^*}{k_B T} = \sum_{j=c,+, -} \frac{n_j}{\Omega} - \frac{\bar{\rho}_p}{b^3} - \ln \frac{1 - \bar{\rho}_p}{b^3} + \frac{\bar{\rho}_p}{N b^3} - \frac{\chi_{ps}}{b^3} \bar{\rho}_p^2, \quad (33)$$

where $\bar{\rho}_p = Nb^3/\Omega$. In the literature⁴¹, osmotic pressure for fluids near surfaces is given by the fluid densities near surfaces (the so called ‘‘contact value theorem’’) and Eq. (32) is nothing but the analog of the ‘‘contact value theorem’’ for the inhomogeneous system *with interactions*.

F. Mean Activity Coefficient

Using the saddle point approximation for the free energy, we have computed the electrostatic chemical potential of small ions. Carrying out the variation of free energy (Eq. (18)) with respect to number of small ions, the mean field estimate for the electrostatic chemical potential¹⁷ of small ions comes out to be

$$\mu_j^{el} = \frac{\delta}{\delta n_j} \left(\frac{F - F_0}{k_B T} \right)_{N, V, n_m \neq j} = \ln \left[\frac{n_j}{\int d\mathbf{r} \exp(-Z_j \psi(\mathbf{r}))} \right] \quad \text{for } j = c, +, -. \quad (34)$$

This is a straightforward generalization of the electrostatic chemical potential for homogeneous system to an inhomogeneous one. Using these expressions, chemical potential for the salt $A_{\nu_+} B_{\nu_-}$ (so that $\nu_+ = \nu_- = 1$ for the monovalent salt) can be written as

$$\mu_{salt} = \nu_+ \mu_+^{el} + \nu_- \mu_-^{el}. \quad (35)$$

However, individual activity coefficients or the chemical potential can not be measured experimentally. So, we construct the mean activity coefficient (γ_{\pm}) for the binary salt¹⁷ defined by

$$\mu_{salt} = \ln \left[\left(\frac{n_+}{\Omega} \right)^{\nu_+} \left(\frac{n_-}{\Omega} \right)^{\nu_-} \gamma_{\pm}^{\nu} \right], \quad (36)$$

where $\nu = \nu_+ + \nu_-$. Using Eq. (35) and (36), mean activity coefficient is given by

$$\gamma_{\pm}^{\nu} = \left[\frac{\Omega}{\int d\mathbf{r} \exp(-Z_+ \psi(\mathbf{r}))} \right]^{\nu_+} \left[\frac{\Omega}{\int d\mathbf{r} \exp(-Z_- \psi(\mathbf{r}))} \right]^{\nu_-}. \quad (37)$$

Using Schwarz’s inequality⁴², it can be shown that the mean activity coefficient is always less than or equal to unity. For the spherical cavity with pure solvent and monovalent salt ions, potential is essentially constant everywhere (local electroneutrality) and that leads to mean activity coefficient being unity. Note that the Eq. (37) can also be derived by considering a Donnan equilibrium between the interior containing polyelectrolyte chain and the exterior containing salt ions with salt concentration c_s .

III. RESULTS

Having presented the field theoretical treatment of a single flexible chain in the presence of solvent, we present the results obtained after solving SCFT equations for a negatively charged chain ($Z_p = -1$) with monovalent salt. In this study, we have taken all small ions (counterions and co-ions) to be point charges and while calculating counterion density profiles, we have added contributions coming from the counterions released by the polyelectrolyte chain and the salt. Also, it should be noticed that due to the point nature of these charges, counterions and co-ions are not excluded from the confining boundary, which can be done, in principle, by the introduction of an arbitrary wall potential⁴³. Here, we simply assume that the *depletion layer*⁴⁴ for counterions and co-ions is very small as compared to the monomer due to an order of difference in their sizes and its negligible effects on the system properties.

All the results reported in this paper have been obtained with a grid spacing of $\Delta r = 0.1$ and chain contour discretization of $\Delta s = 0.01$ after putting $b = 1$ nm.

1. Monomer and charge distribution

To study the effect of confinement, we have varied degree of polymerization (N) keeping all other parameters fixed. Increase in N with fixed R leads to a more confined environment with the increase in monomer density everywhere inside the cavity. This can be seen in Fig. 1, where we have plotted monomer densities for a single polyelectrolyte chain for different values of N after choosing a particular set of parameters ($\chi_{ps} = 0.45, \alpha = 0.1, l_B/b = 0.7, R/b = 5, c_s = 0.1M$). These values for the parameters were chosen to mimic a salty flexible polyelectrolyte chain under spherical confinement in the presence of water as a solvent. Also, for comparison purposes, we have plotted monomer densities for the corresponding neutral chains in an athermal solvent ($\chi_{ps} = 0$) and in an equivalent solvent condition ($\chi_{ps} = 0.45$). Comparing the monomer density for the neutral chain in athermal solvent with a poorer solvent, it is clear that the exclusion of solvent molecules from the core of the coil is stronger as the solvent quality is decreased, as expected. Now, when the polymer in the less good solvent is charged, the solvent exclusion effect is slightly weaker. This difference becomes negligible as the monomer volume frac-

tion increases. Moreover, monomer density profiles for neutral and the polyelectrolyte chain in the same solvent are almost identical, which corroborates the coil conformation of the polyelectrolyte.

We have also varied R by keeping the number of salt ions and α fixed, and the results obtained for radial densities are shown in Fig. 2 for a particular value of N (number of salt-ions corresponds to $c_s = 0.1M$ for $R/b = 5$). The observed difference in small ion density profiles for different R 's is attributed to the fact that total salt concentration (c_s) is changing when R is being changed with the number of small ions kept fixed during this variation. In this figure, we have chosen $N = 100$ and the rest of the parameters are the same as in Fig. 1 for the polyelectrolyte chain. From Fig. 2, it is evident that due to exclusion of the monomers from confining sphere surface, decrease in R leads to an increase in concentration of monomers in the interior. Had it been a bulk situation ($R \rightarrow \infty$), small ion densities would have reached their bulk value (c_s). Looking at small ions' densities in Fig. 2, it is clear that for the confined spherical system, this common presumed result is no more valid and small ion density profiles haven't reached their bulk value. In other words, net radial charge density is no more zero near the confining boundary (as shown in Fig. 3) and a double layer system⁴⁵ is set up as a result of depletion of the chain from the surface.

In this study, small ions are treated as point charges and hence, are not excluded from the surface of the spherical cavity in contrast to the monomer. As a result, when N is increased keeping α fixed at stronger confinements (in terms of higher monomer densities), there are more number of counterions (positively charged) generated by the chain and hence, charge density near the surface of the cavity increases (Fig. 3). On the other hand, near the center of the cavity, the local charge density curves move toward zero as N is increased (i.e. interior of the cavity is becoming locally electroneutral). For lower degrees of confinements (i.e. low $\bar{\rho}_p$), increase in N leads to increase in charge density everywhere due to more number of ions in the system. However, this behavior is seen over a very small density regime.

We have also varied other parameters (c_s , α and l_B). Effects of all these parameters on monomer densities are consistent with the observation that a polyelectrolyte⁶ chain at high salt concentration is equivalent to a neutral chain with an effective excluded volume parameter given by

$$w_{eff} = \frac{1}{1 - \bar{\rho}_p} - 2\chi_{ps} + \frac{4\pi l_B \alpha^2 Z_p^2}{\kappa^2}. \quad (1)$$

So, the polyelectrolyte chain shows higher expansion⁴⁶ as compared to its neutral analog⁴⁷.

On the other hand, at low salt concentrations, the chain can tend to attain a rod-like conformation due to dominance of electrostatic repulsions along the backbone and spherical symmetry is broken. In our mean field study, we use spherical symmetry and Gaussian model for the polyelectrolyte chain. Due to these limitations, spherical symmetry breaks down in the extremely low salt regime and we are not allowed to explore the low salt regime using the current model.

These results show that confinement of the chain leads to the development of a charge density wave inside the cavity and an outcome of this charge density wave is that there is a potential difference across the center of the cavity and the surface. It is to be noted that for a confined system with only small ions inside, potential is constant everywhere and local electroneutrality is the equilibrium state (trivial solution of SCF equations). However, it is the depletion of the chain from the cavity surface, which leads to the accumulation of charges near the surface and as a result inhomogeneous charge distribution is attained. To study the role of polyelectrolyte in the free energy, we compare the free energies of the inhomogeneous phase with the cavity containing pure solvent and salt-ions in the next section.

2. Free energy within saddle point approximation

In Fig. 4, we have plotted different contributions to free energy for a salty system using Eqs. (19 - 23). Analyzing the contributions to free energy, it is clear that the free energy has four major contributions. At lower polymer volume fractions, free energy is dominated by entropy of small ions ($-TS_{ions}/k_B T$) and solvent ($-TS_{solvent}/k_B T$). As volume fraction is increased, chain conformational entropy and polymer-solvent interaction energy also become important. Also, electrostatic energy part in free energy is small compared to other terms, stressing a minor role played by electrostatic energy in the crowded environment under investigation here. Share of each contribution to the free energy depends on the degree of confinement. For instance, when degree of confinement is extremely high ($Nb^3/\Omega \rightarrow 1$), solvent entropy and polymer-solvent interaction energy terms are negligible and free energy

has two major contributions - small ion entropy and chain conformational entropy. Strictly speaking, our theoretical model breaks down as soon as monomer density inside the cavity is close to unity because the finite size of small ions and nature of interactions between the various species become important. All these effects can not be captured with our theory, which involves only two body interaction potential.

A few comments about the shape of the plots in Fig. 4 are due here. Shape of small ions entropy term is governed by number of small ions term ($\sum_j \int d\mathbf{r} \rho_j(\mathbf{r})$ in Eq. (22)) and when N is increased keeping degree of ionization (α) and R fixed, number of counterions increases and hence, $-TS_{ions}/k_B T$ decreases with increase in N (almost linearly). Similarly, when N is increased while keeping R fixed, total number of solvent molecules in the cavity decreases (due to incompressibility) and hence, $-TS_{solvent}/k_B T$ increases. Increase in N for a fixed R/b leads to lower number of conformations available to the chain and hence, entropy of the chain decreases or $-TS_{poly}/k_B T$ increases. Shape of excluded volume interaction energy and electrostatic interaction energy can be understood by the fact that in the asymptotic limit with respect to degree of confinement, the product of densities (monomer and solvent) as well as the electric potential are small.

In implicit solvent computations²⁸, free energy goes linearly with N^2/Ω . In order to see whether the same linear law is followed by free energy in explicit solvent model, we have plotted free energy as a function of N^2/Ω for different values of R/b in Fig. 5. It is found that free energy follows the linear law only for lower values of $\bar{\rho}_p$. For higher $\bar{\rho}_p$, there are deviations from this linear law due to the conformational entropy of the chain. Overall, the shape of the free energy curve is of the form $\sum_{j=c,+,-,s} n_j [\ln(n_j/\Omega) - 1]$ for lower $\bar{\rho}_p$ and systematic deviations are seen for higher $\bar{\rho}_p$.

Also, to highlight the role of the polyelectrolyte in the free energy of confinement, we have plotted the *difference* between the free energy of the spherical cavity with and without chain (i.e. $\Delta F^* = F^* - F\{\bar{\rho}_p = 0\}$) for different radii of the confining cavity and monomer densities in Fig. 6. In these computations, it has been assumed that $w_{pp} = w_{ss}$ to get rid of an uninteresting constant. The results reveal that the confinement of the chain is a thermodynamically unfavorable process and for the same density, larger value of ΔF^* for larger spherical cavity can be attributed to the difference in conformational entropy and polymer-solvent interaction energy for chains of different lengths in spheres of different radii.

In scaling theories²³, it is commonly asserted that the confinement free energy is extensive

in N . In order to confirm this assertion, we have plotted $(F^* - F_0)/Nk_B T$ for various values of monomer densities at different values of R (see Fig. 7). Our results clearly show that the free energy under spherical confinement is not extensive in N , in contrast to the rectangular and cylindrical confinements²³.

3. Osmotic pressure and mean activity coefficient

In Fig. 8, we have plotted the osmotic pressure obtained from Eq. (32) as a function of monomer density. For comparison purposes, we have also plotted the osmotic pressure of the homogeneous phase (Eq. (33)). It is found that the osmotic pressure is the same for the homogeneous and the inhomogeneous phase at lower monomer densities and ideal gas law for osmotic pressure is obtained in this regime. However, at higher densities, deviations from ideal gas law are seen and these deviations are larger for the inhomogeneous phase in comparison with the homogeneous phase. Comparing each term in Eqs. (32) and (33), it is found that the discrepancy between the inhomogeneous and homogeneous phase arises as a result of the depletion of the chain from the spherical surface. Due to the depletion, the monomer density at one Kuhn step away from the surface is higher for the inhomogeneous system in comparison with the homogenous system. Moreover, the log term involving solvent density and quadratic excluded volume interaction term involving the chi parameter add to the discrepancy. Other than these terms, electrostatic and small ions terms do not change much. Effect of the cavity radius on the osmotic pressure profiles can be easily explained using Eq. (33) and the fact that number densities of salt ions is higher for smaller cavity, when number of ions is kept fixed during the computation.

In the absence of the polyelectrolyte, the local electroneutrality is the equilibrium state for the small ions. That means the mean activity coefficient for the salt is unity. However, due to the depletion of the chain from the surface, local electroneutrality gets broken and that leads to a deviation from unity. In Fig. 9, we have plotted the mean activity coefficient for the monovalent salt and it is clear that the presence of the polyelectrolyte chain leads to deviation from ideal behavior (local electroneutrality). The shape of the activity coefficient curves can be understood by the fact that local electroneutrality is attained for very large densities also, where number of small ions is large and almost uniformly distributed. Effect of R on these plots can be explained by the fact that the extent of inhomogeneity in electrostatic

potential increases with an increase in R .

4. One-loop fluctuation corrections : narrow depletion zone approximation

The saddle point approximation used in computing free energy (Eq. (18)) is valid when the number densities of small molecules and monomers is high (i.e. concentrated regime). In order to capture the role of fluctuations in the concentrated regime, we have expanded the integrand of functional integrals over fields around the saddle point solution up to quadratic terms in fields (Appendix-B) so that the functional integrals to be carried out are Gaussian (one-loop calculations). For low concentrations (dilute and semi-dilute regimes), this treatment breaks down and other techniques have to be employed.

Even at the one-loop level, it is very difficult to sum the infinite series, which emerge as a result of Gaussian integrals. Moreover, these sums are plagued with ultraviolet divergences, which have to be regularized. However, we have been able to sum these series in the long chain limit ($N \rightarrow \infty$) when $\kappa R \rightarrow \infty$ and $\xi^{-1}R \rightarrow \infty$, where κ^{-1} and ξ are Debye and Edwards' screening lengths, respectively. In the concentrated regime for a very long chain, the width of the depletion zone near the surface of the sphere is very small as compared to the radius of the sphere and we can suppress the radial dependence of the densities (cf. Fig. 1 and 2). Taking this approximation and ignoring the correlation energy of the charges along the backbone of the chain (which is very small for a weakly charged polyelectrolyte), the free energy at one-loop level can be written as (Appendix-B)

$$\frac{F}{k_B T} = \frac{F^*}{k_B T} + \frac{1}{2} \sum_{k=1}^{\infty} \sum_{l=0}^{\infty} (2l+1) \left[\ln \left(1 + \frac{R^2/\xi^2}{\nu_{kl}^2} \right) + \ln \left(1 + \frac{\kappa^2 R^2}{\nu_{kl}^2} \right) \right], \quad (2)$$

where $\kappa^2 = 4\pi l_B \sum_{c,+,-} Z_j^2 n_j / \Omega$, $\xi^{-2} = 12 \left(\frac{1}{1-\rho_p} - 2\chi_{ps} \right) N b / \Omega$ and ν_{kl} is k^{th} zero of the spherical Bessel function of order l (i.e. $j_l(\nu_{kl}) = 0$). The infinite sum over k can be computed exactly. However, the sum over l diverges. The divergence can be regularized by introducing an upper cutoff M on l and identifying cut-off independent part. The *finite* sum over l has been computed in Ref.³¹. The cut-off independent part gives

$$\frac{F}{k_B T} = \frac{F^*}{k_B T} - \frac{(\kappa^3 + \xi^{-3})\Omega}{12\pi} + \frac{\kappa^2 S}{32\pi} (1 + 2 \ln \kappa R) + \frac{\xi^{-2} S}{32\pi} (1 + 2 \ln \xi^{-1} R) + \frac{1}{3} (\kappa + \xi^{-1}) R, \quad (3)$$

where S is the surface area of the sphere ($= 4\pi R^2$). In the above expression, cubic terms in κ and ξ^{-1} represent the bulk contribution of fluctuations to the free energy and other terms correspond to the finite size corrections, which arise as a result of confinement. Note that for $R \rightarrow \infty$, these finite size contributions vanish and the well-known screening result is obtained. Also, the finite size contributions are smaller than the bulk contributions in the limit discussed here and hence, overall, fluctuations lower the total free energy.

Fluctuation corrections to the osmotic pressure and the mean activity coefficient can be estimated in a straightforward way by using Eq. (3). It must be kept in mind that Eq. (3) is strictly valid in the strong screening regime for an infinitely long chain. In order for these conditions to be realized, spherical cavity has to be very large to accommodate the long chain (because of incompressibility condition). On the other hand, numerical solution of SCF equations for large spherical cavities with a very long chain becomes very expensive. So, in this study, we limit ourselves to a qualitative discussion about the fluctuation corrections to osmotic pressure and mean activity coefficient.

Qualitatively, the osmotic pressure is decreased due to fluctuations (because the fluctuations at one loop level lower the free energy). It can be shown quite easily that the leading corrections to the pressure profiles^{17,18} will be of the form $-\kappa^3/24\pi$ and $-\xi^{-3}/24\pi$. In the thermodynamic limit of infinite volume for an infinitely long chain, these expressions become exact. As the osmotic pressure must be positive, this analysis sets the range of validity of the one-loop calculations¹⁸ to be well above the overlap concentration (in the concentrated regime). In fact, below those concentrations, perturbative treatment to capture the role of fluctuations fails and non-perturbative methods to capture the role of higher order terms in the expansion of the integrand have to be used (e.g. in dilute and semi-dilute regime)^{6,18}.

The finite size corrections to these laws (originating from the last three terms on the right hand side in Eq. 3) are small but positive and overall, increase the range of validity of the fluctuation analysis. Similar analysis can be carried out for the mean-activity coefficient of the monovalent salt and the leading corrections coming from fluctuations¹⁷ are of the form $\exp(-\kappa l_B/2)$. Of course, the analysis is valid for the low salt concentrations (Debye-Hückel regime) because the size and the nature of the short-range interactions of salt ions become important at higher concentrations.

IV. CONCLUSIONS

We have studied a weakly charged flexible polyelectrolyte chain under spherical confinement using SCFT. In Sections II and III, we have demonstrated that SCFT predicts creation of a charge density wave and a potential difference across the center of the sphere and the boundary.

We have also shown that for a given charge density along the backbone, free energy of a flexible chain ($F^* - F_0$) has four major contributions - entropy of small ions, entropy of solvent, energy due to polymer-solvent interactions and conformational entropy of the chain. Share of each contribution to the free energy depends on the monomer density, degree of ionization and salt-concentration inside the sphere. However, electrostatic interaction energy plays a minor role in free energy for the weakly charged flexible polyelectrolyte. Our results show that the free energy is not extensive in the number of monomers.

Osmotic pressure for the polyelectrolyte chain follows ideal gas law in the low monomer density regime and substantial deviations are seen as the monomer density is increased. Mean activity coefficient for the monovalent salt show a small, yet systematic deviation from unity, highlighting the role of the polyelectrolyte in breaking the local electroneutrality condition seen in the absence of the polyelectrolyte.

One-loop fluctuation analysis (within the approximation of narrow depletion zone) reveals that fluctuations lower the free energy and the free energy has additional contributions coming from screening effects due to monomers as well as small-ions. Without any confinement, the fluctuations corrections at one-loop level¹⁸ have been shown to lower the free energy and the range of validity of the fluctuation analysis is set by the condition that osmotic pressure must be positive. The concentrations over which the condition is satisfied, come out to be well-above the overlap concentration in polymer solution theories. As the finite size corrections to the fluctuation contributions in the free energy are positive, so the range of validity of the fluctuation analysis gets widened due to the confinement.

Finally, we comment on the assumptions used in arriving at the above conclusions:

(1) We have used the spherical symmetry of the system which is valid as long as coil conformation of the chain is retained and a rod like conformation is avoided. Also, we have used SCFT for a flexible polyelectrolyte chain, which means the chain must not be stiffened due to charges on the backbone and large torsional barriers. These criteria are realized in

the presence of high salt, where electrostatic interactions get screened and become short ranged.

(2) Saddle-point approximation breaks down in the extremely dilute limit for monomers, solvent and small-ions. The approximation is strictly valid in the concentrated regime in the presence of enough salt and solvent. The necessity to have many solvent molecules, sets upper limit to be away from extremely dense regime, where $Nb^3/\Omega \rightarrow 1$.

In this study, fluctuations in densities and fields about the mean field solution of SCF equations have been treated perturbatively by expanding free energy functional up to quadratic order about the saddle point. This fluctuation analysis breaks down for low density regime, where higher order terms also contribute and need to be taken into account using an appropriate non-perturbative treatment.

(3) Role of solvent is taken into account by taking the volume of a solvent molecule as the same as that of a monomer. In reality, solvent size may be smaller than Kuhn step length and incompressibility constraint is violated near the boundary. For the present study, we have simply assumed that the effect of the depletion zone for solvent on the system properties is negligible and can be ignored. All these limitations of the current model can be removed by taking the solvent size to be different from the monomer⁴⁸ and using $\rho_p(r) + \rho_s(r) = \rho(r)$, where $\rho(r)$ is a suitable function, which is ρ_0 away from the boundary and falls from ρ_0 to zero in a smooth fashion within the depletion zone⁴⁸. However, the choice of $\rho(r)$ and width of depletion zone is arbitrary and depends on the numerics of the problem.

Similarly, small ions have been treated as point charges, which might not be a bad approximation knowing the fact that typical ion radii for monovalent cations and anions lie in the range $\sim 0.06 - 0.22$ nm⁴⁹.

(4) In principle, the degree of ionization (α) should also be computed by minimization of free energy⁵⁰ with respect to α . In order to simplify the numerical work, we have taken the degree of ionization (α) to be independent of l_B and avoided any ion condensation effects.

(5) While splitting the free energy into energy and entropy, we have assumed that dielectric constant (ϵ) of the solvent is insensitive to temperature. However, the temperature

dependence of the dielectric constant^{38,51} can be easily incorporated in our theory.

ACKNOWLEDGEMENT

We acknowledge financial support from NIH Grant 5R01HG002776-05, NSF Grant No. DMR 0605833, and the Material Research Science and Engineering Centre at the University of Massachusetts, Amherst.

APPENDIX A : SCFT with explicit solvent

Here, we present a summary of the steps in obtaining the saddle point equations for a single polyelectrolyte chain in the presence of salt ions and solvent molecules (section (II A)). The procedure is similar to the ones presented in Refs.^{35,36}. As the first step, we define microscopic densities as

$$\hat{\rho}_p(\mathbf{r}) = \frac{1}{b} \int_0^{Nb} ds \delta(\mathbf{r} - \mathbf{R}(s)) \quad (\text{A-1})$$

$$\hat{\rho}_j(\mathbf{r}) = \sum_{i=1}^{n_j} \delta(\mathbf{r} - \mathbf{r}_i) \quad \text{for } j = s, c, +, - \quad (\text{A-2})$$

$$\hat{\rho}_e(\mathbf{r}) = e \left[\alpha Z_p \hat{\rho}_p(\mathbf{r}) + \sum_{j=c,+, -} Z_j \hat{\rho}_j(\mathbf{r}) \right], \quad (\text{A-3})$$

where $\hat{\rho}_p(\mathbf{r})$, $\hat{\rho}_j(\mathbf{r})$ and $\hat{\rho}_e(\mathbf{r})$ stand for monomer, small molecules (ions and solvent molecules) and local charge density, respectively.

As the second step, we use a functional integral representation for the incompressibility constraint

$$\prod_r \delta(\hat{\rho}_p(\mathbf{r}) + \hat{\rho}_s(\mathbf{r}) - \rho_0) = \int D[w_+(\mathbf{r})] e^{-i \int d\mathbf{r} w_+(\mathbf{r})(\hat{\rho}_p(\mathbf{r}) + \hat{\rho}_s(\mathbf{r}) - \rho_0)}, \quad (\text{A-4})$$

where $w_+(\mathbf{r})$ is the well-known pressure field which enforces the incompressibility constraint at all points in the system and $i = \sqrt{-1}$.

As the third step, dimensionless Flory's chi parameter is introduced to club together the three excluded volume parameters so that

$$\chi_{ps} b^3 = w_{ps} - \frac{w_{pp} + w_{ss}}{2}. \quad (\text{A-5})$$

Note that the clubbing of excluded volume parameters has been possible because of the incompressibility constraint so that only one independent parameter appears in the theory. Otherwise, there would have been three independent parameters.

Following these three steps, Eq. (1) becomes

$$\begin{aligned} \exp\left(-\frac{F}{k_B T}\right) &= \frac{1}{\prod_j n_j!} \int D[\mathbf{R}] \int \prod_j \prod_{m=1}^{n_j} d\mathbf{r}_m \int D[w_+(\mathbf{r})] \exp\left\{-\frac{3}{2b} \int_0^{N_b} dt \left(\frac{\partial \mathbf{R}(t)}{\partial t}\right)^2\right. \\ &\quad -i \int d\mathbf{r} w_+(\mathbf{r}) (\hat{\rho}_p(\mathbf{r}) + \hat{\rho}_s(\mathbf{r}) - \rho_0) - \chi_{ps} b^3 \int d\mathbf{r} \hat{\rho}_p(\mathbf{r}) \hat{\rho}_s(\mathbf{r}) \\ &\quad \left. - \frac{1}{2} \int d\mathbf{r} \int d\mathbf{r}' \frac{\hat{\rho}_e(\mathbf{r}) \hat{\rho}_e(\mathbf{r}')}{\epsilon k_B T |\mathbf{r} - \mathbf{r}'|}\right\} \exp\left\{-\frac{\rho_0}{2} (N w_{pp} + n_s w_{ss})\right\}. \end{aligned} \quad (\text{A-6})$$

So far, we have written the partition function in terms of the local densities. Now, we want to write this partition function in terms of the order parameter of the system. There are many different choices we can make for the order parameter^{52,53}. However, in this study, we follow the method as described in ref.⁵³ to introduce the order parameter. As the fourth step, we define

$$\hat{\rho}_+(\mathbf{r}) = \hat{\rho}_p(\mathbf{r}) + \hat{\rho}_s(\mathbf{r}) = \rho_0 \quad (\text{A-7})$$

$$\hat{\rho}_-(\mathbf{r}) = \hat{\rho}_p(\mathbf{r}) - \hat{\rho}_s(\mathbf{r}), \quad (\text{A-8})$$

where $\hat{\rho}_-(\mathbf{r})$ is the order parameter for the inhomogeneous system.

As the fifth step, to go from densities to fields, we use the Hubbard-Stratonovich transformation for short range excluded volume interactions as well as long range electrostatic interactions, so that

$$\exp\left(\frac{\chi_{ps} b^3}{4} \int d\mathbf{r} \hat{\rho}_-^2(\mathbf{r})\right) = \frac{1}{\mu_-} \int D[w_-(\mathbf{r})] \exp\left[\int d\mathbf{r} \left\{w_-(\mathbf{r}) \hat{\rho}_-(\mathbf{r}) - \frac{1}{\chi_{ps} b^3} w_-^2(\mathbf{r})\right\}\right], \quad (\text{A-9})$$

$$\exp\left(-\frac{1}{2} \int d\mathbf{r} \int d\mathbf{r}' \frac{\hat{\rho}_e(\mathbf{r}) \hat{\rho}_e(\mathbf{r}')}{\epsilon k_B T |\mathbf{r} - \mathbf{r}'|}\right) = \frac{1}{\mu_\psi} \int D[\psi(\mathbf{r})] \exp\left[-\int d\mathbf{r} \left\{i\psi(\mathbf{r}) \frac{\hat{\rho}_e(\mathbf{r})}{e} - \frac{\psi(\mathbf{r})}{8\pi l_B} \nabla_{\mathbf{r}}^2 \psi(\mathbf{r})\right\}\right], \quad (\text{A-10})$$

where

$$\mu_- = \int D[w_-(\mathbf{r})] \exp\left[-\frac{1}{\chi_{ps} b^3} \int d\mathbf{r} w_-^2(\mathbf{r})\right] \quad (\text{A-11})$$

$$\mu_\psi = \int D[\psi(\mathbf{r})] \exp\left[\frac{1}{8\pi l_B} \int d\mathbf{r} \psi(\mathbf{r}) \nabla_{\mathbf{r}}^2 \psi(\mathbf{r})\right]. \quad (\text{A-12})$$

Note that, $w_+(\mathbf{r})$, $w_-(\mathbf{r})$ and $\psi(\mathbf{r})$ are the *real* fields, which can be envisioned as chemical potential fields³⁷. Now, taking these two steps, Eq. (A-6) becomes

$$\exp\left(-\frac{F}{k_B T}\right) = \frac{1}{\mu - \mu_\psi} \int D[w_+(\mathbf{r})] \int D[w_-(\mathbf{r})] \int D[\psi(\mathbf{r})] \exp[-f\{w_+, w_-, \psi\}], \quad (\text{A-13})$$

where

$$\begin{aligned} f\{w_+, w_-, \psi\} = & \frac{1}{\chi_{ps} b^3} \int d\mathbf{r} w_-^2(\mathbf{r}) - i\rho_0 \int d\mathbf{r} w_+(\mathbf{r}) - \ln Q_p - \sum_{j=s,c,+,-} n_j \ln Q_j \\ & - \frac{1}{8\pi l_B} \int d\mathbf{r} \psi(\mathbf{r}) \nabla_{\mathbf{r}}^2 \psi(\mathbf{r}) + \frac{\rho_0}{2} \left(N w_{pp} + n_s w_{ss} + \frac{\chi_{ps} b^3}{2} \Omega \rho_0 \right) \\ & + \sum_{j=s,c,+,-} \ln n_j! \end{aligned} \quad (\text{A-14})$$

$$Q_p = \int D[\mathbf{R}(t)] \exp \left[-\frac{1}{b} \int_0^{Nb} dt \left\{ \frac{3}{2} \left(\frac{\partial \mathbf{R}}{\partial t} \right)^2 + i w_+ \{\mathbf{R}\} - w_- \{\mathbf{R}\} + i Z_p \alpha \psi \{\mathbf{R}\} \right\} \right] \quad (\text{A-15})$$

$$Q_s = \int d\mathbf{r} \exp[-\{i w_+(\mathbf{r}) + w_-(\mathbf{r})\}] \quad (\text{A-16})$$

$$Q_j = \int d\mathbf{r} \exp[-i Z_j \psi(\mathbf{r})] \quad \text{for } j = c, +, -. \quad (\text{A-17})$$

The functional integrations over real fields are to be carried out by contour integration techniques and are almost impossible to compute exactly. However, if the number of small molecules is large then we can compute the integrals in the numerator by steepest descent technique, using the knowledge that the integral along the constant phase (imaginary part of the integrand) contour is dominated by the local minima of the integrand⁵³ (note that the functional integrals in the denominator are divergent and ignored at the level of saddle point approximation). So, we approximate the functional integrals in the numerator by the value of the integrand at the local minima (where the phase comes out to be zero) so that the final approximated integral is real ($= f\{w_+^*, w_-^*, \psi^*\}$). However, the saddle point values for w_+ ($= w_+^*$) and ψ ($= \psi^*$) come out to be purely imaginary in contrast to w_- ($= w_-^*$), which is real.

Also, it should be noted that the densities remain unchanged with the shift in fields by an arbitrary constant. So, we write $i w_+(\mathbf{r}) - \frac{1}{2} \chi_{ps} b^3 \rho_0 = i w_+(\mathbf{r})$ to get rid of the constant

in saddle point equations. Now, deriving local minima equations for the integrand in Eq. (A-14) with respect to w_+ , w_- and ψ , and using notation $iw_+(\mathbf{r}) - w_-(\mathbf{r}) \rightarrow \phi_p(\mathbf{r})$, $iw_+(\mathbf{r}) + w_-(\mathbf{r}) \rightarrow \phi_s(\mathbf{r})$, $i\psi(\mathbf{r}) \rightarrow \psi(\mathbf{r})$, $iw_+(\mathbf{r}) \rightarrow \eta(\mathbf{r})$, Eqs. (7-13) are obtained. Using these saddle point equations and employing Stirling's approximation for $\ln n!$, we obtain Eq. (18).

APPENDIX B : Fluctuations around the saddle point

Here, we provide details for one loop treatment of the fluctuations³⁴. We expand the integrand f in Eq. (A-13) up to second degree terms in w_+ , w_- and ψ around their respective saddle point values. For convenience in writing the expansion, we introduce a dummy functional variable $\zeta_p(\mathbf{r})$, where $p = 1, 2, 3$ correspond to w_+ , w_- and ψ , respectively. In this notation, the expression for free energy becomes (cf. Eq. (A-13))

$$\exp\left(-\frac{F - F^*}{k_B T}\right) = \frac{1}{\mu_- \mu_\psi} \int \prod_{p=1}^3 D[\zeta_p(\mathbf{r})] \exp\left[-\frac{1}{2} \int d\mathbf{r} \int d\mathbf{r}' \sum_{m=1}^3 \sum_{p=1}^3 K_{mp}(\mathbf{r}, \mathbf{r}') (\zeta_m(\mathbf{r}) - \zeta_m^*(\mathbf{r}')) (\zeta_p(\mathbf{r}) - \zeta_p^*(\mathbf{r}'))\right], \quad (\text{B-1})$$

where

$$K_{mp}(\mathbf{r}, \mathbf{r}') = \frac{\delta^2 f \{\zeta_1, \zeta_2, \zeta_3\}}{\delta \zeta_m(\mathbf{r}) \delta \zeta_p(\mathbf{r}')} \Big|_{\zeta_1^*, \zeta_2^*, \zeta_3^*}. \quad (\text{B-2})$$

In the expansion, linear terms in fields vanish because of the saddle point condition. K_{mp} can be computed in a straightforward way and are presented here for completeness

$$K_{11}(\mathbf{r}, \mathbf{r}') = A(\mathbf{r}, \mathbf{r}') + B_s(\mathbf{r}, \mathbf{r}') \quad (\text{B-3})$$

$$K_{22}(\mathbf{r}, \mathbf{r}') = C(\mathbf{r}, \mathbf{r}') - A(\mathbf{r}, \mathbf{r}') - B_s(\mathbf{r}, \mathbf{r}') \quad (\text{B-4})$$

$$K_{33}(\mathbf{r}, \mathbf{r}') = -\frac{1}{4\pi l_B} \nabla_{\mathbf{r}}^2 \delta(\mathbf{r} - \mathbf{r}') + Z_p^2 \alpha^2 A(\mathbf{r}, \mathbf{r}') + \sum_{j=e,+,-} Z_j^2 B_j(\mathbf{r}, \mathbf{r}') \quad (\text{B-5})$$

$$K_{12}(\mathbf{r}, \mathbf{r}') = K_{21}(\mathbf{r}, \mathbf{r}') = i[A(\mathbf{r}, \mathbf{r}') - B_s(\mathbf{r}, \mathbf{r}')] \quad (\text{B-6})$$

$$K_{13}(\mathbf{r}, \mathbf{r}') = K_{31}(\mathbf{r}, \mathbf{r}') = Z_p \alpha A(\mathbf{r}, \mathbf{r}') \quad (\text{B-7})$$

$$K_{23}(\mathbf{r}, \mathbf{r}') = K_{32}(\mathbf{r}, \mathbf{r}') = i Z_p \alpha A(\mathbf{r}, \mathbf{r}') \quad (\text{B-8})$$

where

$$A(\mathbf{r}, \mathbf{r}') = -\rho_p(\mathbf{r}) \rho_p(\mathbf{r}') + g(\mathbf{r}, \mathbf{r}') \quad (\text{B-9})$$

$$g(\mathbf{r}, \mathbf{r}') = \left[\int_0^N ds' \int_0^{s'} ds q(\mathbf{r}, s) G(\mathbf{r}, \mathbf{r}', s, s') q(\mathbf{r}', N - s') \right. \\ \left. + \int_0^N ds \int_0^s ds' q(\mathbf{r}', s') G(\mathbf{r}', \mathbf{r}, s', s) q(\mathbf{r}, N - s) \right] \frac{1}{\int d\mathbf{r} q(\mathbf{r}, N)} \quad (\text{B-10})$$

$$B_j(\mathbf{r}, \mathbf{r}') = -\frac{1}{n_j} \rho_j(\mathbf{r}) \rho_j(\mathbf{r}') + \rho_j(\mathbf{r}) \delta(\mathbf{r} - \mathbf{r}') \quad \text{for } j = s, c, +, - \quad (\text{B-11})$$

$$C(\mathbf{r}, \mathbf{r}') = \frac{2}{\chi_{ps} b^3} \delta(\mathbf{r} - \mathbf{r}'). \quad (\text{B-12})$$

In the case of confined chain within a spherical cavity, where electrostatic potential and monomer density are zero at the boundary (Dirichlet boundary conditions), the functional integral over ζ_p can be carried out in Eq. (B-1) by expanding all vectorial quantities in terms of spherical harmonics (Y_{lm}) and spherical Bessel functions (j_l). For an arbitrary function $h(\mathbf{r}, \mathbf{r}')$ this means

$$h(\mathbf{r}, \mathbf{r}') = \sum_{k=1}^{\infty} \sum_{l=0}^{\infty} \sum_{m=-l}^l h_{kl} d_{kl}(r) d_{kl}(r') Y_{lm}(\theta, \phi) Y_{lm}^*(\theta', \phi') \quad (\text{B-13})$$

$$d_{kl}(r) = \sqrt{\frac{2}{3}} \frac{j_l(\nu_{kl} r / R)}{|j_{l+1}(\nu_{kl})|}, \quad (\text{B-14})$$

where ν_{kl} is k^{th} zero of the spherical Bessel function of order l (i.e. $j_l(\nu_{kl}) = 0$). Similarly, we expand $\zeta_p(\mathbf{r})$ as

$$\zeta_p(\mathbf{r}) = \sum_{k=1}^{\infty} \sum_{l=0}^{\infty} \sum_{m=-l}^l \zeta_{pk} d_{kl}(r) Y_{lm}(\theta, \phi). \quad (\text{B-15})$$

Now, using orthogonal properties of spherical Bessel and spherical harmonics, the functional integrals can be computed. After some lengthy algebra,

$$\frac{F}{k_B T} = \frac{F^*}{k_B T} + \frac{1}{2} \sum_{k=1}^{\infty} \sum_{l=0}^{\infty} (2l+1) \ln \left(A_{kl} + B_{s,kl} - 4 \sum_{u=1}^{\infty} \sum_{v=1}^{\infty} A_{ku} C_{uv}^{-1} B_{s,vl} \right) \\ + \frac{1}{2} \sum_{k=1}^{\infty} \sum_{l=0}^{\infty} (2l+1) \ln \left(1 + \frac{4\pi l_B R^2}{\nu_{kl}^2} \sum_{j=c,+, -} Z_j^2 B_{j,kl} \right) \\ + \frac{1}{2} \sum_{k=1}^{\infty} \sum_{l=0}^{\infty} (2l+1) \ln \left(1 + Z_p^2 \alpha^2 \frac{A_{kl} - \sum_{u=1}^{\infty} \sum_{v=1}^{\infty} A_{ku} L_{uv}^{-1} A_{vl}}{\frac{\nu_{kl}^2}{4\pi l_B R^2} + \sum_{j=c,+, -} Z_j^2 B_{j,kl}} \right). \quad (\text{B-16})$$

In the above equation, the second term on the r.h.s. represents the contribution of correlations arising due to excluded volume interactions between monomers (neutral polymer contribution), the third term arises as a result of small-ions density fluctuations and the last term correctly represents the correlation energy of charges along the backbone of the chain.

Also, C_{kl}^{-1} and L_{kl}^{-1} correspond to the coefficients in the spherical harmonics expansion for the inverse operator of $C(\mathbf{r}, \mathbf{r}')$ and $L(\mathbf{r}, \mathbf{r}')$, respectively. Inverse operator for any arbitrary functional $h(\mathbf{r}, \mathbf{r}')$ is defined by

$$\int d\mathbf{r}' h(\mathbf{r}, \mathbf{r}') h^{-1}(\mathbf{r}', \mathbf{r}'') = \delta(\mathbf{r} - \mathbf{r}''), \quad (\text{B-17})$$

which gives $\sum_{u=1}^{\infty} h_{ku} h_{ul}^{-1} = \delta_{kl}$, where δ_{kl} is Kronecker delta. Also, $L(\mathbf{r}, \mathbf{r}')$ is given by

$$L(\mathbf{r}, \mathbf{r}') = A(\mathbf{r}, \mathbf{r}') + B(\mathbf{r}, \mathbf{r}') + 4 \int d\mathbf{r}'' \int d\mathbf{r}''' B(\mathbf{r}, \mathbf{r}'') (C - 4B)^{-1}(\mathbf{r}'', \mathbf{r}''') B(\mathbf{r}''', \mathbf{r}'). \quad (\text{B-18})$$

Unfortunately, computation of the coefficients involved in Eq. (B-16) requires three dimensional calculations for the densities and it is very hard to compute the sums exactly, which diverge in general. To gain an insight into the problem, we have identified one particular case, where we can evaluate the first two terms analytically.

If the number of small molecules (solvent and small ions) is large, then operators $B_j(\mathbf{r}, \mathbf{r}')$ become diagonal and also, number densities ($\rho_j(\mathbf{r})$) show a weak dependence on \mathbf{r} . Similarly, if degree of polymerization N is large (strictly if $N \rightarrow \infty$), then monomer density becomes independent of \mathbf{r} except near the surface of the cavity characterized by the width of the depletion zone, which can be neglected. If both of these conditions are satisfied, then suppressing position dependence of densities, we get

$$\begin{aligned} \frac{1}{2} \sum_{k=1}^{\infty} \sum_{l=0}^{\infty} (2l+1) \ln \left(A_{kl} + B_{s,kl} - 4 \sum_{u=1}^{\infty} \sum_{v=1}^{\infty} A_{ku} C_{uv}^{-1} B_{s,vl} \right) &= \frac{1}{2} \sum_{k=1}^{\infty} \sum_{l=0}^{\infty} (2l+1) \ln(1 - \bar{\rho}_p) \\ &+ \frac{1}{2} \sum_{k=1}^{\infty} \sum_{l=0}^{\infty} (2l+1) \ln(1 + w_r b^3 A_{kl}), \end{aligned} \quad (\text{B-19})$$

where $\bar{\rho}_p = \frac{Nb^3}{\Omega}$ and $w_r = \frac{1}{1-\bar{\rho}_p} - 2\chi_{ps}$ is the renormalized excluded volume interaction parameter. For constant monomer density (while working in the limit $N \rightarrow \infty$), $A(\mathbf{r}, \mathbf{r}')$ satisfies

$$\nabla_{\mathbf{r}}^2 A(\mathbf{r}, \mathbf{r}') = -\frac{12N}{b^2\Omega} \delta(\mathbf{r} - \mathbf{r}') \quad (\text{B-20})$$

so that $b^3 A_{kl} = 12NbR^2/(\nu_{kl}^2\Omega)$. Neglecting the correlation energy of the charges along the backbone of the chain (the last term on r.h.s. of Eq. (B-16)) and an ultraviolet divergent sum in Eq. (B-19) (first term on r.h.s. of the equation), Eq. (2) is obtained.

REFERENCES

- ¹ P.G. de Gennes, P. Pincus, R.M. Velasco, F. Brochard, *Journal de Physique* **37**, 1461 (1976).
- ² A.R. Khokhloy, *J.Phys.A: Math. Gen.* **13**, 979 (1980).
- ³ M. Muthukumar, *J. Chem. Phys.* **86**, 7230 (1987).
- ⁴ V.Yu. Borue and I.Ya. Erukhimovich, *Macromolecules* **21**, 3240 (1988).
- ⁵ J.F. Marko and Y. Rabin , *Macromolecules* **24**, 2134 (1991); *ibid.* **25**, 1503 (1992).
- ⁶ M. Muthukumar , *J. Chem. Phys.* **105**, 5183 (1996).
- ⁷ K.K. Mahdi, M. de la Cruz, *Macromolecules* **33**, 7649 (2000).
- ⁸ M. Muthukumar, *Macromolecules* **35**, 9142 (2002).
- ⁹ K. Ghosh, G.A. Carri and M. Muthukumar, *J. Chem. Phys.* **116**, 5299 (2002).
- ¹⁰ C. Holm, J.F. Joanny, K. Kremer, R.R. Netz, P. Reineker, C. Seidel, T.A. Vilgis, R.G. Winkler, *Advances in Polymer Science* **166**, 67 (2004).
- ¹¹ K. Nishida, K. Kaji and T. Kanaya, *J. Chem. Phys.* **114**, 8671 (2001).
- ¹² K. Nishida, K. Kaji and T. Kanaya, *J. Chem. Phys.* **115**, 8217 (2001).
- ¹³ L. Zhang and A. Eisenberg, *Science* **268**, 1728 (1995); L. Zhang and A. Eisenberg, *Macromolecules* **29**, 8805 (1996); K. Yu and A. Eisenberg, *Macromolecules* **31**, 3509 (1998).
- ¹⁴ S.A. Jenekhe and X.L. Chen, *Science* **279**, 1903 (1998).
- ¹⁵ V.M. Prabhu, M. Muthukumar, G.D. Wignall, Y.B. Melnichenko, *J. Chem. Phys.* **119**, 4085 (2003).
- ¹⁶ S. Forster, V. Abetz, A.H.E. Muller, *Advances in Polymer Science* **166**, 173 (2004).
- ¹⁷ D.A. McQuarie, *Statistical Mechanics* (University Science Books, Sausalito, California, 20 00).
- ¹⁸ M. Doi and S.F. Edwards, *The Theory of Polymer Dynamics* (Clarendon Press, Oxford, 1986).
- ¹⁹ R.T. Fraley, S.L. Dellaporta, D. Papahadjopoulos, *PNAS* **79**,1859 (1982).
- ²⁰ J. J. Kasianowicz, E. Brandin, D. Branton, and D. W. Deamer, *PNAS* **93**, 13770 (1996).
- ²¹ M. Akeson, D. Branton, J. J. Kasianowicz, E. Brandin, and D. W. Deamer, *Biophys. J.* **77**, 3227 (1999).
- ²² R.J. Murphy and M. Muthukumar, *J. Chem. Phys.* **126**, 051101 (2007).
- ²³ P . G. de Gennes,*Scaling Concepts in Polymer Physics* (Cornell University Press, Ithaca and

- London, 1979).
- ²⁴ Y. Chen and M. Muthukumar, Phys. Rev. B **33**, 6187 (1986).
- ²⁵ A.Y. Grosberg and A. R. Khokhlov, *Statistical Physics of Macromolecules* (American Institute of Physics, New York, 1994).
- ²⁶ A. Cacciuto and E. Luijten, Nano Lett. **6**, 901 (2006).
- ²⁷ A. Cacciuto and E. Luijten, Phys. Rev. Lett. **96**, 238104 (2006).
- ²⁸ C. Y. Kong and M. Muthukumar, J. Chem. Phys. **120**, 3460 (2004).
- ²⁹ W. Sung and P. J. Park, Phys. Rev. Lett. **77**, 783 (1996).
- ³⁰ M. Muthukumar, J. Chem. Phys. **118**, 5174 (2003).
- ³¹ A. Torres and G. Téllez, J. Stat. Phys. **118**, 735 (2005).
- ³² M. Muthukumar and S.F. Edwards, J. Chem. Phys. **76**, 2720 (1982).
- ³³ J. des Cloizeaux and G. Jannink, *Polymers in Solution* (Clarendon Press, Oxford, 1990).
- ³⁴ K.F. Freed, *Renormalization Group Theory of Macromolecules* (Wiley, New York, 1987).
- ³⁵ A. Shi and J. Noolandi, Macromol. Theory Simul. **8**, 214 (1999).
- ³⁶ Q. Wang, T. Takashi, and G.H. Fredrickson, J. Phys. Chem. B **108**, 6733 (2004).
- ³⁷ E. Helfand, J. Chem. Phys. **62**, 999 (1975).
- ³⁸ R. A. Marcus, J. Chem. Phys. **23**, 1057 (1955).
- ³⁹ W.H. Press, S.A. Teukolsky, W.T. Vetterling and B. P. Flannery, *Numerical Recipes in C* (Cambridge University Press , New York, 1992).
- ⁴⁰ M. Muthukumar and J. S. Ho, Macromolecules **22**, 965 (1989).
- ⁴¹ R. Podgornik, J. Phys. Chem. **97**, 3927 (1993).
- ⁴² I.S. Gradshteyn and I.M. Ryzhik , *Tables of Integrals, Series, and Products* (Academic Press,San Diego, 2000).
- ⁴³ S. Tsonchev, R. D. Coalson, and A. Duncan, Phys. Rev. E **60**, 4257 (1999).
- ⁴⁴ G . J. Fleer, M.A.Cohen Stuart, J.M.H.M. Scheutjens, T. Cosgrove and B. Vincent, *Polymers at Interfaces* (Chapman & Hall, London, 1993).
- ⁴⁵ E.J.W. Verwey and J.T.G.Overbeek, *Theory of The Stability of Lyophobic Colloids* (Dover Publications, Inc., New York, 1999).
- ⁴⁶ M. Beer, M. Schmidt, and M. Muthukumar, Macromolecules **30**, 8375 (1997).
- ⁴⁷ M. Muthukumar and B. G. Nickel, J. Chem. Phys. **86**, 460 (1987).
- ⁴⁸ J.R. Naughton and M.W. Matsen, Macromolecules **35**, 5688 (2002); M.W. Matsen, J. Chem.

- Phys. **106**, 7781 (1997).
- ⁴⁹ J.N. Israelachvili, *Intermolecular and Surface Forces* (Academic Press, London, 1991).
- ⁵⁰ M. Muthukumar, J. Chem. Phys. **120**, 9343 (2004).
- ⁵¹ J.T.G. Overbeek, Colloids Surf. **51**, 61 (1990).
- ⁵² T. Ohta and K. Kawasaki, Macromolecules **19**, 2621 (1986).
- ⁵³ G.H. Fredrickson, *The Equilibrium Theory of Inhomogeneous Polymers* (Oxford University, New York, 2006).

FIGURE CAPTION

- Fig. 1.:** Effect of N on monomer densities - comparison with the corresponding neutral chains . In above plots, we have chosen $R/b = 5$ and $N = 100, N = 200$ and $N = 300$ from bottom to top, respectively .
- Fig. 2.:** Effect of cavity radius (R) on ion densities. In these plots, we have chosen $N = 100, \alpha = 0.1, l_B/b = 0.7, \chi_{ps} = 0.45$ and number of salt ions is kept fixed (in all these plots, number of salt ions is equivalent to salt concentration of $0.1M$ for a sphere of radius $R/b = 5$). Solid, dashed and dash-dotted lines represent $\rho(r) = \alpha\rho_p(r), \rho_c(r) + \rho_+(r)$ and $\rho_-(r)$, respectively.
- Fig. 3.:** Effect of cavity radius (R) on net charge density, $\rho_e(r) = \sum_{j=c,+,-} Z_j\rho_j(r) + Z_p\alpha\rho_p(r)$. In these plots, we have chosen $\alpha = 0.1, l_B/b = 0.7, \chi_{ps} = 0.45$ and number of salt ions is kept fixed (in all these plots, number of salt ions is equivalent to salt conc of $0.1M$ for sphere of radius $R/b = 5$). N is increased in steps of 50 starting from 50.
- Fig. 4.:** Different contributions to the free energy within the saddle point approximation for salty systems. Here, we have chosen $N = 100, \alpha = 0.1, l_B/b = 0.7, \chi_{ps} = 0.45, c_s = 0.1M, R/b = 5$.
- Fig. 5.:** Effect of confinement on the free energy within the saddle point approximation. Here, we have chosen $\alpha = 0.1, l_B/b = 0.7, \chi_{ps} = 0.45$ and number of salt ions is kept fixed so that the number of salt ions is equivalent to salt concentration of $0.1M$ for sphere of radius $R/b = 5$.
- Fig. 6.:** Difference in free energy of the spherical cavity with and without polyelectrolyte chain, $\Delta F^* = F^* - F\{\bar{\rho}_p = 0\}$. All other parameters are the same as in Fig. 5.
- Fig. 7.:** Non-extensive nature of free energy of confinement. Parameters are the same as in Fig. 5.
- Fig. 8.:** Comparison between osmotic pressure for the confined polyelectrolyte chain and the homogeneous phase (cf. Eq. (33)). Solid lines correspond to the inhomogeneous case and dashed lines represent the homogeneous system. Parameters are the same as in Fig. 5.

Fig. 9.: Mean activity coefficients for monovalent salt as a function of monomer density of the polyelectrolyte. For comparison purposes, parameters have been chosen to be the same as in Fig. 5.

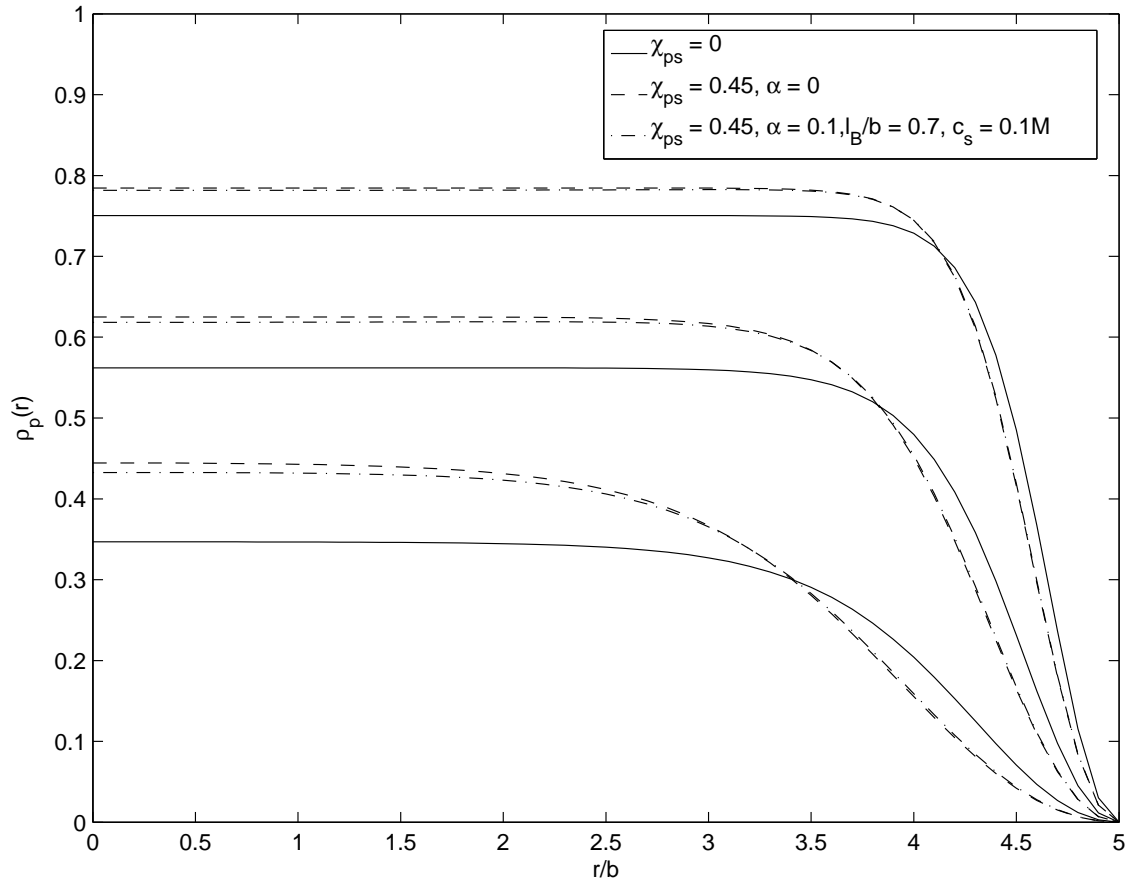


FIG. 1:

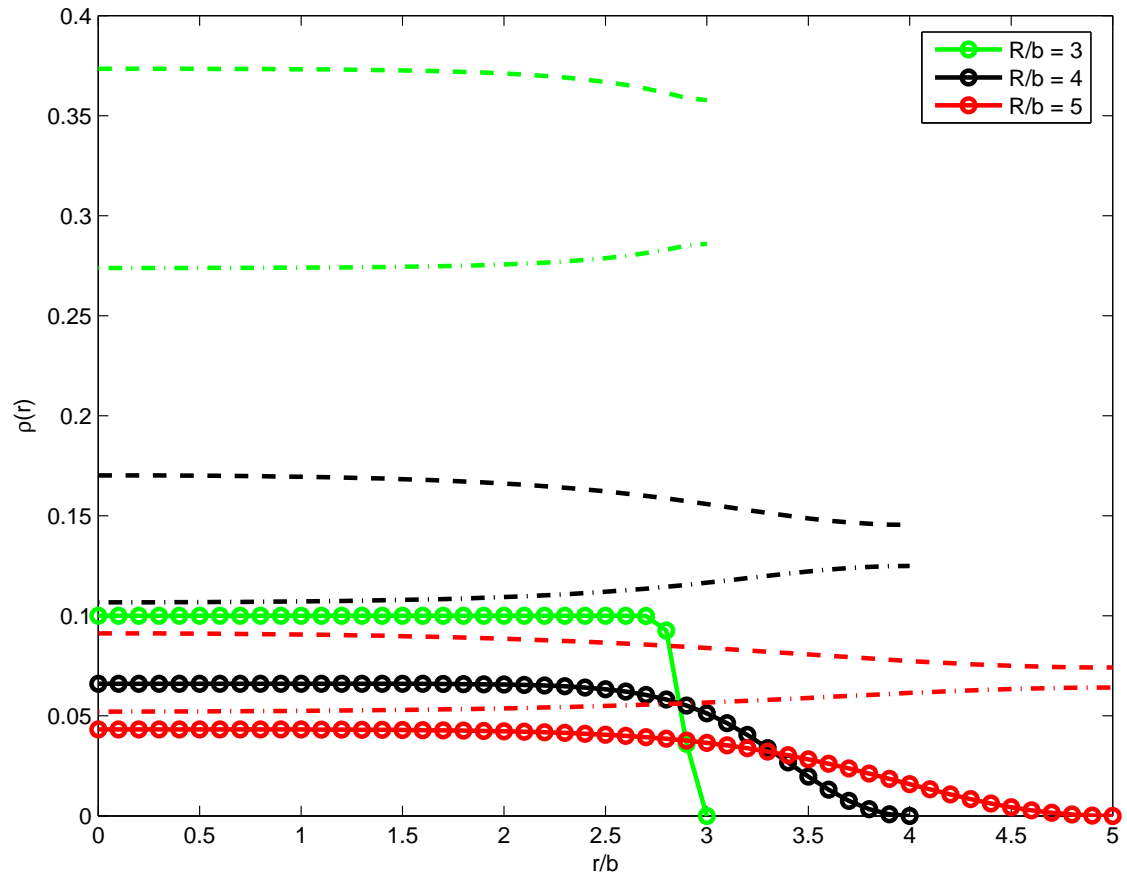


FIG. 2:

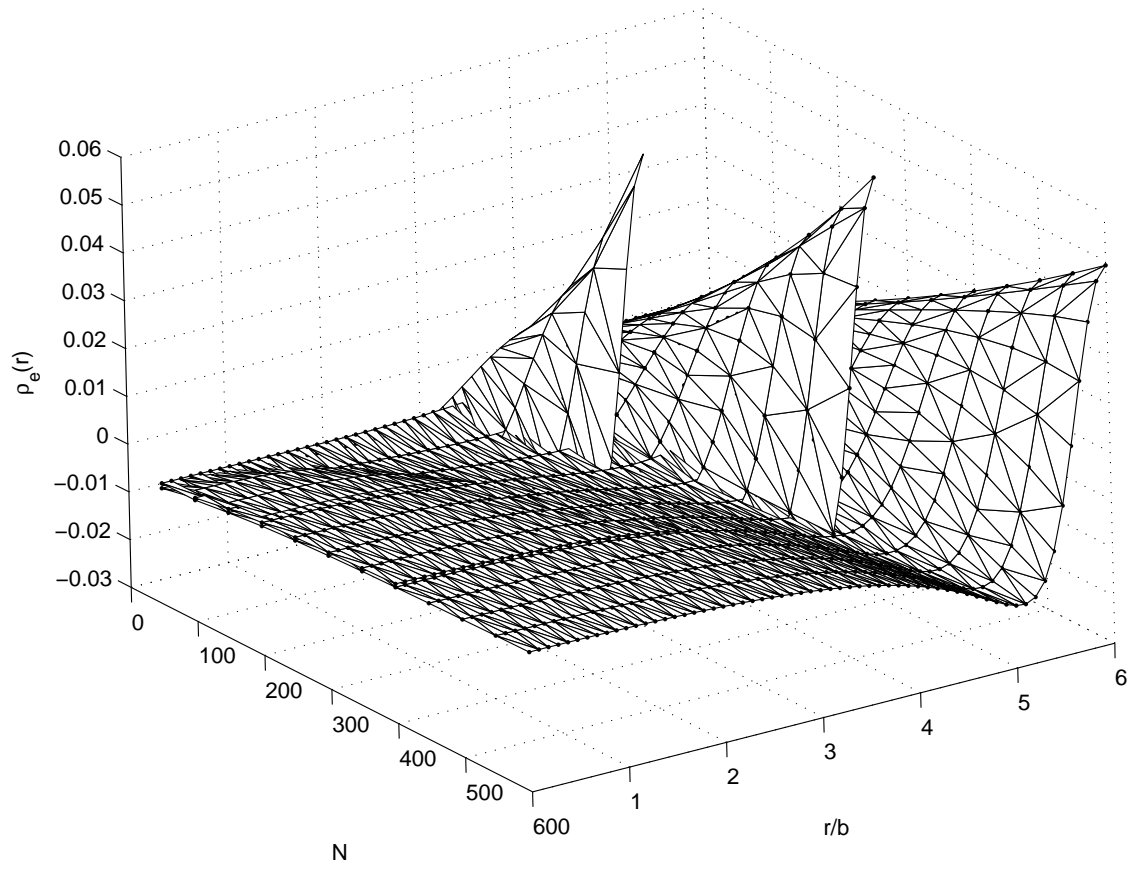


FIG. 3:

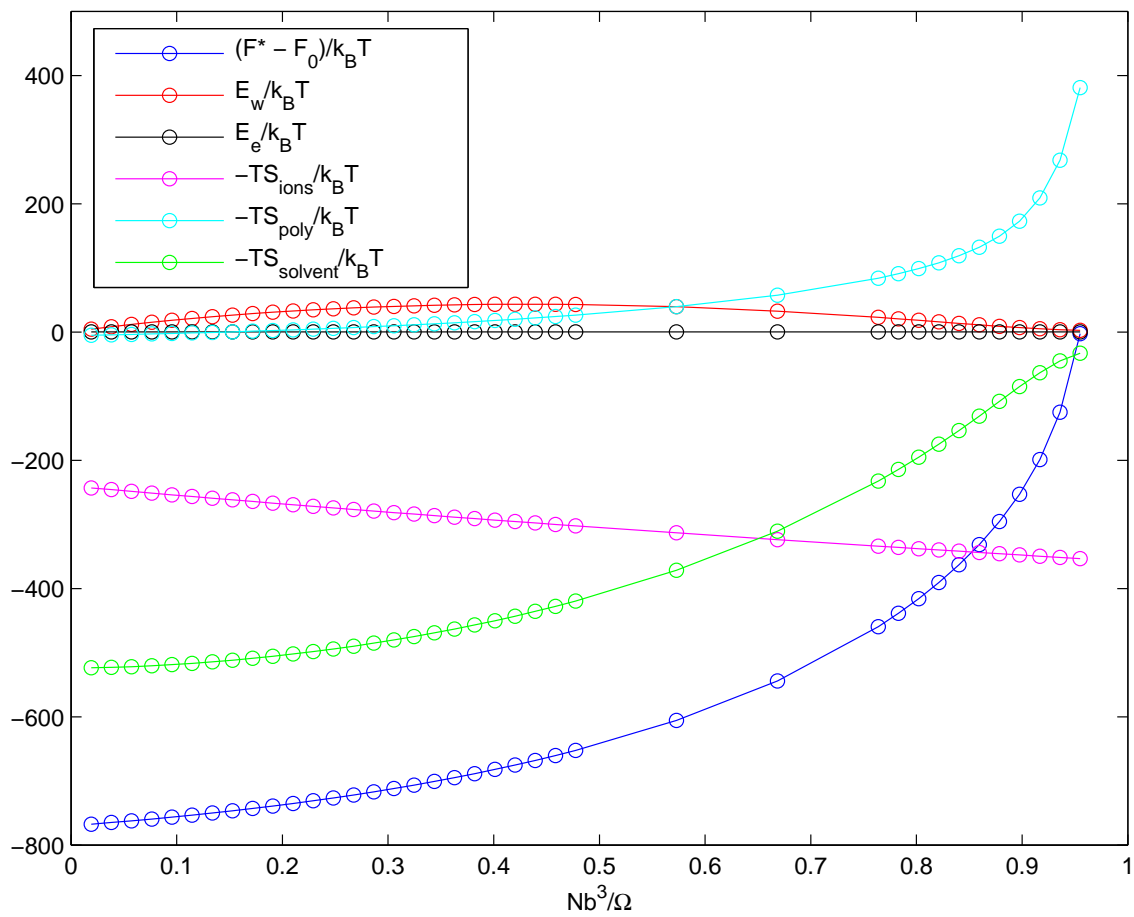


FIG. 4:

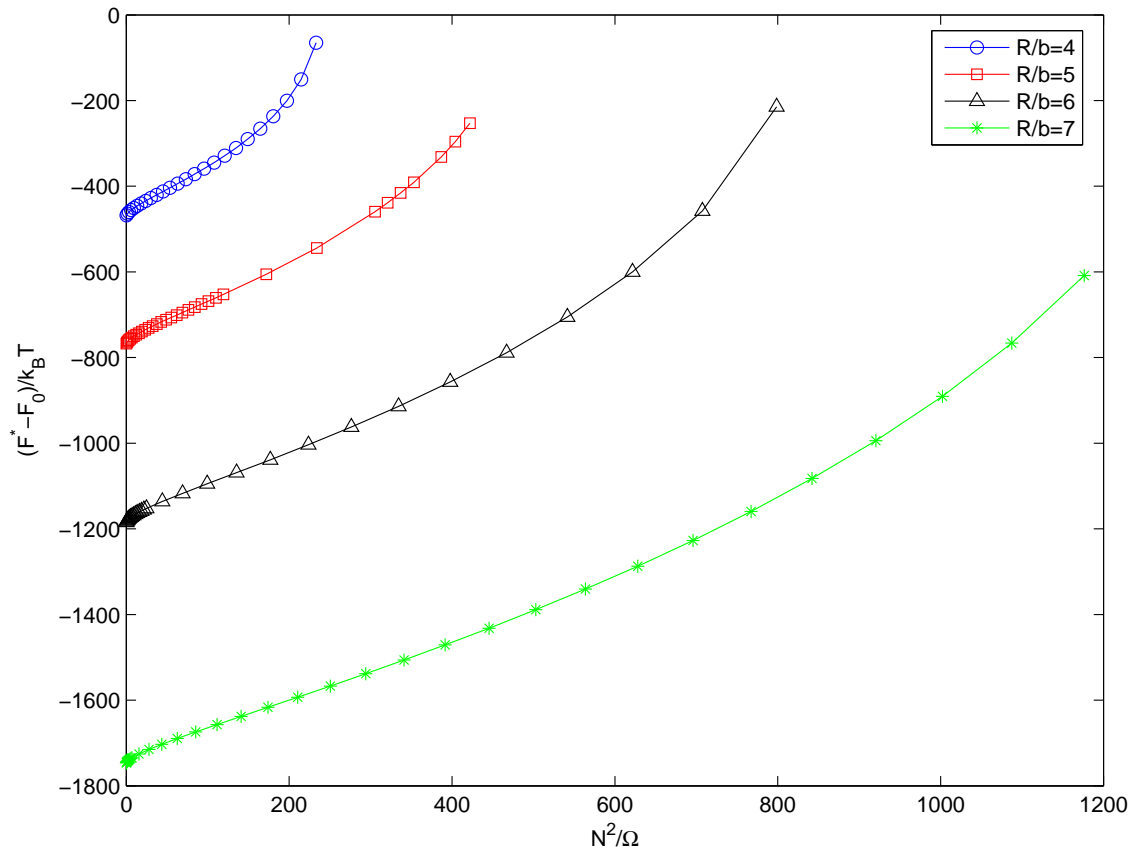


FIG. 5:

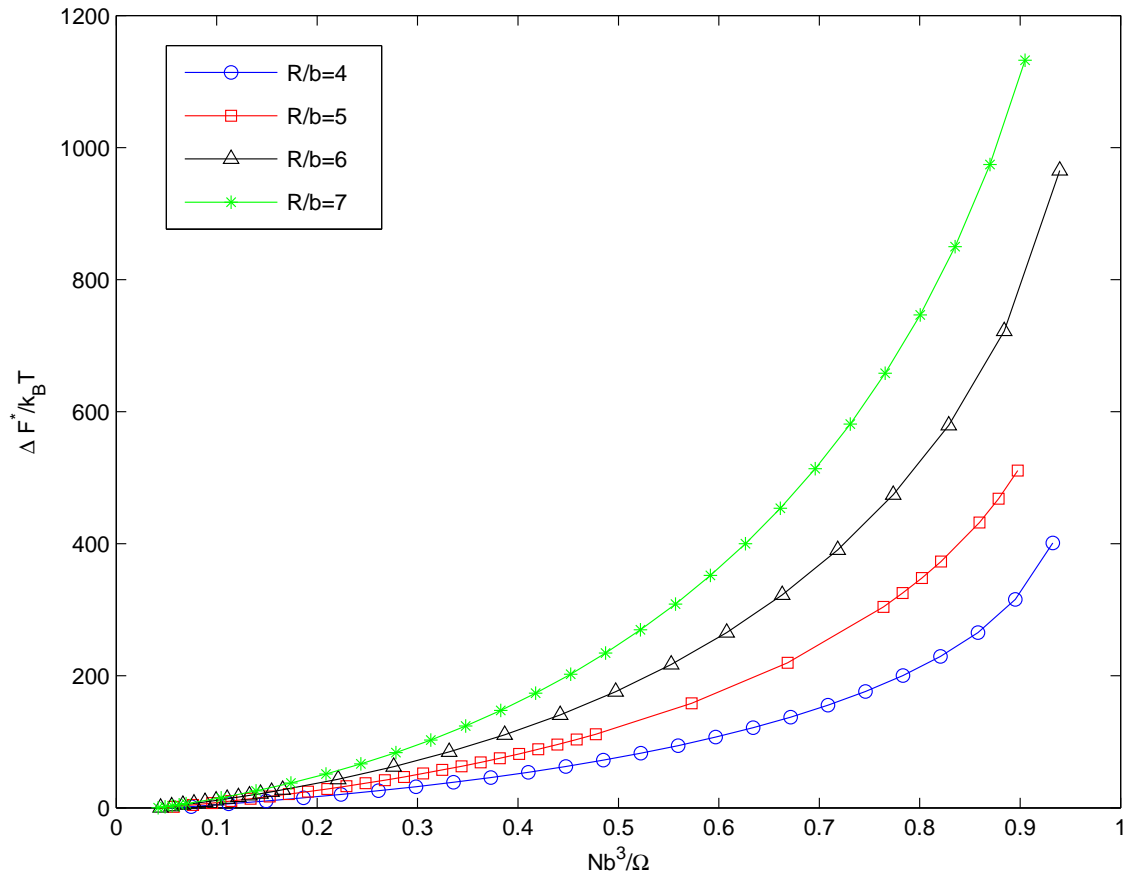


FIG. 6:

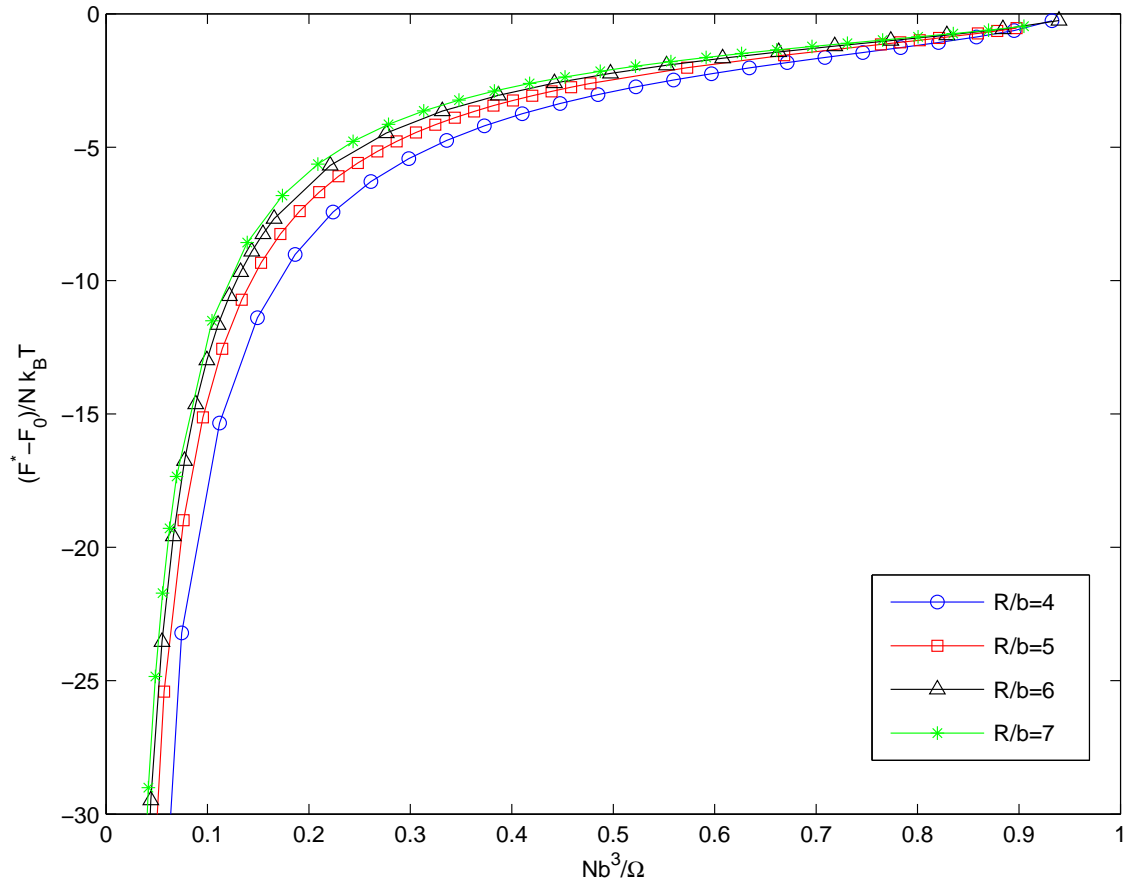


FIG. 7:

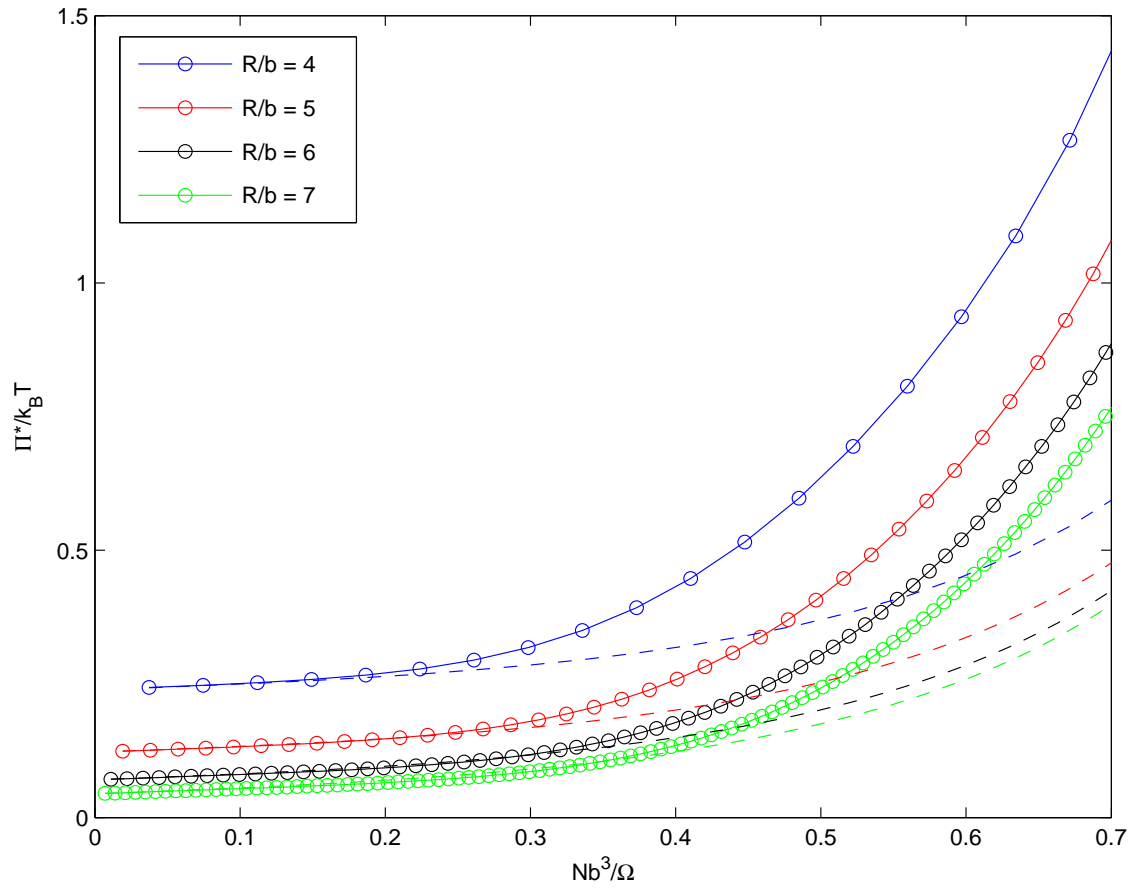


FIG. 8:

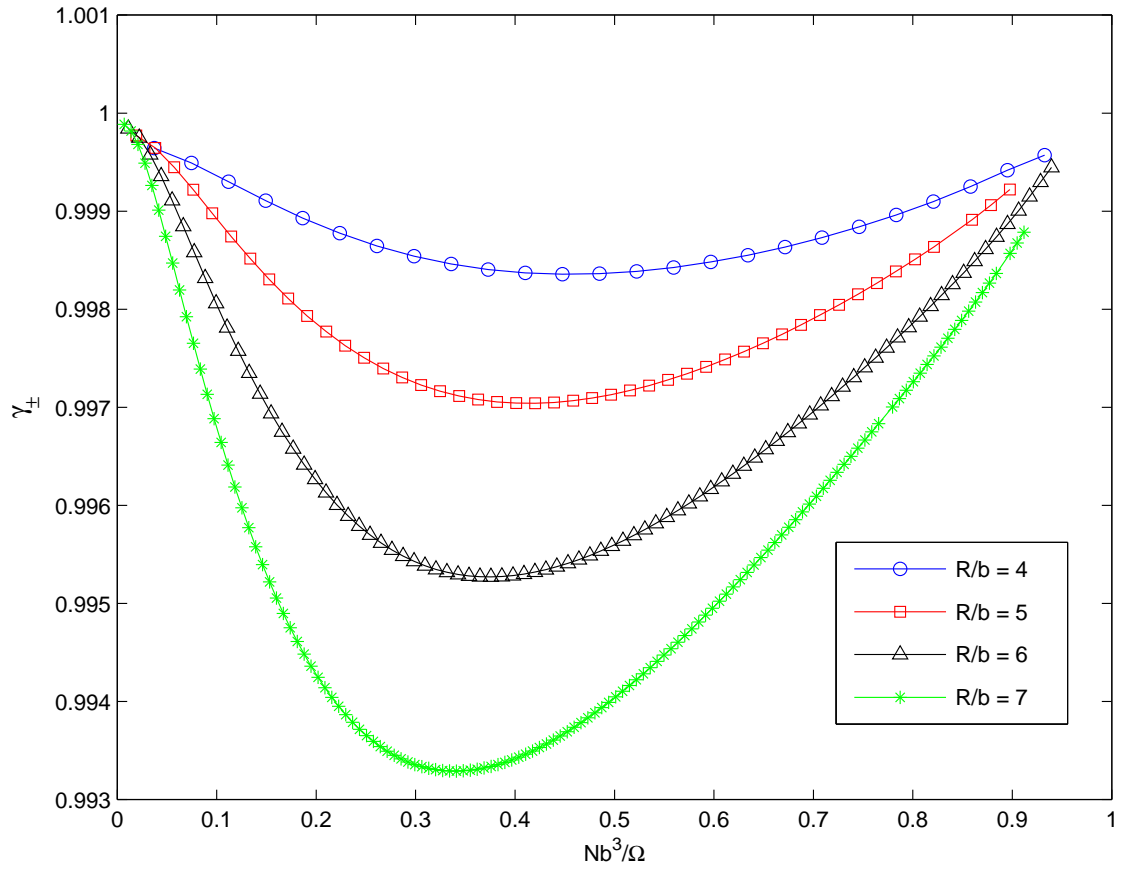


FIG. 9: